Quasilinear modelling of RMP interaction with a tokamak plasma: application to ASDEX Upgrade ELM mitigation experiments

2014 Nucl. Fusion 54 064005

(http://iopscience.iop.org/0029-5515/54/6/064005)

IOP Publishing | International Atomic Energy Agency Nuclear Fusion
Nucl. Fusion **54** (2014) 064005 (17pp) doi:10.1088/0029-5515/54/6/064005

Quasilinear modelling of RMP interaction with a tokamak plasma: application to ASDEX Upgrade ELM mitigation experiments

Martin F. Heyn[1], Ivan B. Ivanov[1,3,4], Sergei V. Kasilov[1,2], Winfried Kernbichler[1], Peter Leitner[1], Viktor V. Nemov[1,2], Wolfgang Suttrop[5] and the ASDEX Upgrade Team[5]

[1] Association EURATOM-ÖAW, Institut für Theoretische Physik—Computational Physics, TU Graz, Petersgasse 16, A-8010 Graz, Austria
[2] Institute of Plasma Physics, National Science Center 'Kharkov Institute of Physics and Technology', Ul. Akademicheskaya 1, 61108 Kharkov, Ukraine
[3] St Petersburg State University, Institute of Physics, Ulyanovskaya 1, Petrodvoretz, 198504, Russia
[4] Petersburg Nuclear Physics Institute, 188300, Gatchina, Leningrad Region, Russia
[5] Max-Planck-Institut für Plasmaphysik, EURATOM Association, D-85748 Garching, Germany

Received 13 July 2013, revised 9 October 2013
Accepted for publication 14 November 2013
Published 23 May 2014

Abstract
First experiments on edge-localized mode (ELM) mitigation with the help of ITER-like coils on ASDEX Upgrade are analysed using linear and quasilinear kinetic models to describe the interaction of resonant magnetic field perturbations (RMP) with the plasma. The gyrokinetic derivation of RMP-driven transport coefficients is given in detail. The role of fluid resonances is studied, in particular the role of the resonance associated with the equilibrium electric field reversal point $E_r = 0$. Like the electron fluid resonance associated with the zero of the total perpendicular electron fluid velocity, the $E_r = 0$ resonance may lead to enhanced transport due to the reduction of RMP shielding in the pedestal region where the RMP field can even be amplified by this resonance. The conditions on the RMP coil spectrum resulting from the analysis are discussed.

Keywords: RMPs, ELM mitigation, tokamak

(Some figures may appear in colour only in the online journal)

1. Introduction

The use of non-axisymmetric external resonant magnetic field perturbations (RMPs) to control edge-localized modes (ELMs) has been successfully demonstrated in DIII-D [1], JET [2] and other devices. This method is foreseen to be used in ITER [3] in order to avoid peak heat loads on the divertor produced by type-I ELMs. Recently, experiments on ELM mitigation using a set of ITER-like coils have been started on ASDEX Upgrade [4, 5]. The analysis of a few first experimental shots using the linear kinetic model of RMP penetration into a plasma developed in [6, 7] and the quasilinear model introduced in [8] is one of the main purposes of this paper.

An overview of the history of ELM mitigation by RMPs with main emphasis on the development of theory and the relevant numerical models can be found in [9] published recently. Since this reference contains a detailed analysis of various theoretical approaches and the relevant literature, the reader is referred to it for details. Here we summarize just a few important steps in the development of the theoretical understanding of ELM mitigation mechanisms. The mechanism as originally suggested by the authors of the first experiments [1] assumed the control of the pedestal pressure with the help of an enhanced transport in the ergodic magnetic field region formed there by externally applied RMPs. In [10] it has been found that the behaviour of the electron temperature in low-collisionality DIII-D shots cannot be explained by various magnetohydrodynamic (MHD) and kinetic transport models using the assumption that the RMP field is the vacuum field. Subsequently, it has been shown by a few models, in particular by the kinetic model of this

paper, that RMPs are strongly shielded in the low-collisional DIII-D plasma and this shielding eliminates the ergodic layer in the main plasma volume and in most of the pedestal region except for a narrow region around the separatrix [11]. At this point, the potential mechanism to explain ELM mitigation in low-collisionality discharges has essentially become unclear.

At the same time, it has long been known [12] and observed in various models, in particular in the model of this paper, that the strong shielding of the perturbations by the plasma may be strongly reduced at fluid resonances, in particular in situations where the total perpendicular electron fluid velocity is zero in the reference frame where the RMP is static. Actually, such a point was present in the core plasma in the shot studied in [11] and one of the perturbation modes nearby this point was observed not to be shielded. At that time, the data on plasma rotation were not so complete, in particular data on the poloidal rotation were missing in [11] and, therefore, the poloidal rotation velocity was set to zero. Recently, the rotation velocity profiles in the DIII-D discharge 126006 studied in [11] have been re-considered by Joseph [13] using a more adequate data analysis. There it has been found that the zero of the perpendicular electron fluid rotation $V_{\perp e} = 0$ and the electric field reversal point $E_r = 0$ are actually located close to or within the pedestal region. This finding was an important step because the possible candidate for the ELM mitigation mechanism in the pertinent experiment has thus been identified.

In [9, 14] it was shown that quasilinear effects of the perturbation mode experiencing the $V_{\perp e} = 0$ resonance can modify the pressure profile in order to mitigate ELMs and cause the experimentally observed density pump-out in long mean free path discharges. At the same time, the second fluid resonance $E_r = 0$ was ruled out in [9] based on arguments that it is removed by anomalous transport. Since both resonances are actually observed in ASDEX Upgrade experiments investigated here, the validity of this conclusion is reviewed in this paper using the kinetic approach.

It should be noted that the kinetic approach of this paper in most cases agrees with the prediction of two-fluid models. At the moment, the kinetic model is still limited in terms of device geometry and the possibility of modelling non-linear effects. In this respect fluid models are more advanced (see, e.g., [15, 16]) but the kinetic model has two other important advantages. First, it suffers less from validity limitations imposed on fluid models in hot, nearly collisionless plasmas, and, second, it allows for an easier interpretation of the results bringing the observed phenomena down to the particle motion level. Some of such interpretations are given in this paper.

The structure of the paper is as follows. In section 2 the linear and quasilinear models of RMP interaction with the plasma are described, in particular, a gyrokinetic derivation of the quasilinear transport equations is given in detail in section 2.1. The linear model is briefly discussed in section 2.2, balance equations are introduced in section 2.3, and the use of the models in a real tokamak geometry is described in section 2.4. In section 3 the DIII-D shot considered in [11] is revisited and compared with ASDEX Upgrade shots. The role of fluid resonances, in particular the role of the equilibrium electric field reversal $E_r = 0$, is discussed in section 4. Requirements to the RMP coil spectrum following from the analysis of this paper are discussed in section 5.

2. Physical model

As in [6, 7, 11], quasilinear and linear theories are constructed in sections 2.1 and 2.2 by modelling the tokamak as a straight radially inhomogeneous cylinder with rotational transform. Cylindrical coordinates (r, ϑ, z) are the radius, azimuthal angle and coordinate along the cylinder axis. The z coordinate is related to the toroidal angle and the major radius of the torus, φ and R, respectively, by $z = R\varphi$. Consequently, the wave number of the perturbation field is linked to the toroidal wave number m_φ by $k_z = m_\varphi R^{-1}$ and the azimuthal component of the equilibrium magnetic field is linked to the z-component by $B_0^\vartheta = B_0^z (qR)^{-1}$ where $q = q(r)$ is the safety factor.

2.1. Quasilinear transport model

Analogous to neoclassical transport theory, the starting point is the gyrokinetic equation written in terms of invariants of motion, the total energy w and the perpendicular adiabatic invariant $J_\perp = m v_\perp^2 (2\omega_c)^{-1}$,

$$\hat{L}_g f \equiv \frac{\partial f}{\partial t} + \boldsymbol{v}_g \cdot \nabla f - \hat{L}_c f = 0. \tag{1}$$

Here, $\boldsymbol{v}_g$ is the guiding centre drift velocity:

$$\boldsymbol{v}_g = \frac{v_\parallel}{B} \nabla \times \left(\boldsymbol{A} + \frac{v_\parallel}{\omega_c} \boldsymbol{B} \right), \tag{2}$$

where

$$v_\parallel = \sigma \sqrt{\frac{2}{m} (w - e\Phi - \omega_c J_\perp)}, \tag{3}$$

with σ the sign of parallel velocity. The curl in (2) is computed assuming w and $J_\perp$ constant.

Note that it is sufficient to use in (2) the magnetic field module B instead of $B_\parallel^*$ introduced in [17] because corrections to the parallel velocity of the order of the guiding centre drift should be ignored when constructing the transport theory. Moreover, the magnetic drift within the flux surface is also ignored in the present model in favour of the $\boldsymbol{E} \times \boldsymbol{B}$ drift, which exceeds the magnetic drift roughly by a factor of the order of the aspect ratio.

Coulomb collisions are represented by an integro-differential model operator

$$\hat{L}_c = \hat{L}_{cD} + \hat{L}_{cI}. \tag{4}$$

The differential part is an Ornstein–Uhlenbeck operator

$$\hat{L}_{cD} f = \nu v_T^2 \frac{\partial}{\partial v_\parallel} \left(\frac{\partial f}{\partial v_\parallel} + \frac{v_\parallel}{v_T^2} f \right), \tag{5}$$

with constant collision frequency ν and thermal velocity $v_T = \sqrt{T/m}$. The integral part is

$$\hat{L}_{cI} f_1(v_\perp, v_\parallel) = \frac{\nu}{\sqrt{2\pi} v_T} \exp\left(-\frac{v_\parallel^2}{2v_T^2} \right) \left(\frac{v_\parallel^2}{v_T^2} - 1 \right) \times \int_{-\infty}^{\infty} \mathrm{d}v'_\parallel \left(\frac{v'^2_\parallel}{v_T^2} - 1 \right) f_1(v_\perp, v'_\parallel). \tag{6}$$

The model operator (4) conserves particles and species energy (heat exchange between species is an effect of the order of

m_e/m_i and is therefore ignored) but does not conserve the parallel momentum. This is done on intention: since the geometry here is a straight cylinder, it does not take into account the parallel flow braking by toroidicity in a real tokamak. This is a result of collisional particle exchange between passing and trapped particles, which are blocked in the parallel direction. Roughly, the parallel flow braking time described by operator (4) is the collision time and is of the same order as the collision time in a real tokamak in the long mean free path regime.

Since, in the present calculations, the expansion parameter is the perturbation electromagnetic field amplitude (in contrast to neoclassical theory where the radial drift velocity is used as an expansion parameter), it is more convenient to sacrifice the compact form of the gyrokinetic equation (1) to an equation in terms of velocity components $v_\perp$ and $v_\parallel$ because the Jacobian of these variables is independent of the electromagnetic field. As a result, on the left-hand side of (1) terms representing the mirroring force appear

$$\hat{L}_g f = \frac{\partial f}{\partial t} + \boldsymbol{v}_g \cdot \nabla f + \dot{v}_\perp \frac{\partial f}{\partial v_\perp} + \dot{v}_\parallel \frac{\partial f}{\partial v_\parallel} - \hat{L}_c f, \qquad (7)$$

described by

$$\dot{v}_\perp = \frac{v_\perp}{2B} \boldsymbol{v}_g \cdot \nabla B, \quad \dot{v}_\parallel = -\frac{e}{m v_\parallel} \boldsymbol{v}_g \cdot \nabla \Phi - \frac{v_\perp^2}{2 v_\parallel B} \boldsymbol{v}_g \cdot \nabla B. \quad (8)$$

Presenting the magnetic field and the electrostatic potential as the sum of equilibrium (labelled with 0) and perturbation fields,

$$\boldsymbol{B} = \boldsymbol{B}_0 + \boldsymbol{B}_1, \qquad \Phi = \Phi_0 + \Phi_1, \qquad (9)$$

we expand the drift velocity, the mirroring force and the distribution function in orders of the perturbation field amplitude,

$$\boldsymbol{v}_g = \boldsymbol{v}_{g0} + \boldsymbol{v}_{g1} + \cdots, \quad \dot{v}_\perp = (\dot{v}_\perp)_0 + (\dot{v}_\perp)_1 + \cdots, \quad \text{etc.} \quad (10)$$

The expansion of the drift velocity is performed assuming $v_\perp$ and $v_\parallel$ to be independent variables. Thus, the steady-state equation (1) is split into a hierarchy

$$\hat{L}_{g0} f_0 = 0,$$

$$\hat{L}_{g0} f_1 = -\boldsymbol{v}_{g1} \cdot \nabla f_0 - (\dot{v}_\perp)_1 \frac{\partial f_0}{\partial v_\perp} - \left(\dot{v}_\parallel\right)_1 \frac{\partial f_0}{\partial v_\parallel}, \quad \ldots, \quad (11)$$

where the operator $\hat{L}_{g0}$ is given by (7) without the time derivative (steady state), with zero-order drift velocity and the mirroring force given in straight cylinder geometry by

$$\boldsymbol{v}_{g0} = \boldsymbol{h} v_\parallel + \boldsymbol{v}_E, \qquad (\dot{v}_\perp)_0 = \left(\dot{v}_\parallel\right)_0 = 0, \qquad (12)$$

where

$$\boldsymbol{h} = \frac{\boldsymbol{B}_0}{B_0}, \qquad \boldsymbol{v}_E = \frac{c}{B_0} \boldsymbol{h} \times \nabla \Phi_0. \qquad (13)$$

Note that in contrast to the neoclassical toroidal viscosity (NTV) theory [18, 19], which also deals with a small perturbation field, the present expansion is performed with respect to unperturbed magnetic surfaces. Therefore, one should formally consider in the particle and energy fluxes

$$\Gamma = \frac{1}{S} \int_S \mathrm{d}S \int \mathrm{d}^3 p \;\; f \, v_g^r, \qquad (14)$$

$$Q = \frac{1}{S} \int_S \mathrm{d}S \int \mathrm{d}^3 p \;\; (w - e\Phi_0) \, f \, v_g^r, \qquad (15)$$

with the drift velocity component normal to the unperturbed flux surfaces

$$v_g^r = \boldsymbol{v}_g \cdot \nabla r, \qquad (16)$$

all second-order terms because the linear order terms vanish during integration over the flux surface area S. Then the zero order distribution function in the form of a local Maxwellian,

$$f_0 = \frac{n_0(r)}{(2\pi m T(r))^{3/2}} \exp\left(-\frac{m\left(v_\perp^2 + v_\parallel^2\right)}{2T(r)}\right) \qquad (17)$$

$$= \frac{n_0(r)}{(2\pi m T(r))^{3/2}} \exp\left(-\frac{w - e\Phi_0(r) - e\Phi_1(r,\vartheta,z)}{T(r)}\right),$$

satisfying the first of (11) can formally contribute to the fluxes in the second order. The use of perturbed surfaces does not make much sense because, in contrast to NTV theory, the perturbed electromagnetic field in the resonant layer does not satisfy the ideal MHD equilibrium where the perturbed equipotential surfaces coincide with the perturbed magnetic surfaces. Actually, as shown below, the mismatch between those surfaces is the main drive for the transport in resonant layers discussed in this study.

The hierarchy (11) can, nevertheless, be broken after the first order since f_2 does not contribute to the fluxes because $v_{g0}^r = 0$ due to (12) where the magnetic drift, which has been ignored, is within the flux surface in the case of a straight cylinder. In addition, it can be shown with the help of (2) that in any geometry the particle flux through any closed surface (which need not be the magnetic flux surface) is identically zero if the distribution function depends on integrals of motion only. This is also true for the total energy flux, which is defined through the total particle energy w and the part of the electrostatic potential constant on the flux surface, Φ_0, as in equation (15). (Such a definition is mandatory in cases where the electrostatic potential is not constant on the unperturbed flux surface because the kinetic energy is not preserved within the flux surface.) Expanding now the local Maxwellian (17) expressed through the integrals of motion up to a linear order over Φ_1 (the only quantity varying on the unperturbed flux surface), one obtains for particle and energy fluxes in the leading order

$$\Gamma = \frac{1}{S} \int_S \mathrm{d}S \int \mathrm{d}^3 p \;\; \tilde{f} \; \boldsymbol{v}_{g1} \cdot \nabla r, \qquad (18)$$

$$Q = \frac{1}{S} \int_S \mathrm{d}S \int \mathrm{d}^3 p \;\; (w - e\Phi) \, \tilde{f} \; \boldsymbol{v}_{g1} \cdot \nabla r, \qquad (19)$$

where

$$\tilde{f} = f_1 + f_0 \frac{e\Phi_1}{T} \qquad (20)$$

satisfies

$$\hat{L}_{g0} \tilde{f} = -\left(A_1 + \frac{m\left(v_\perp^2 + v_\parallel^2\right)}{2T} A_2\right) f_0 \, v_{g1}^r. \qquad (21)$$

Here, the thermodynamic forces are

$$A_1 = \frac{1}{n}\frac{\partial n}{\partial r} + \frac{e}{T}\frac{\partial \Phi_0}{\partial r} - \frac{3}{2T}\frac{\partial T}{\partial r}, \qquad A_2 = \frac{1}{T}\frac{\partial T}{\partial r}, \qquad (22)$$

and the radial drift velocity is

$$v^r_{g1} = \frac{B^r_1}{B_0} v_\parallel - \frac{c}{B_0 r}\left(h_z \frac{\partial \Phi_1}{\partial \vartheta} - h_\vartheta \frac{\partial \Phi_1}{\partial z}\right) + \frac{v_\parallel^2}{\omega_{c0} B_0 r}\left(\frac{\partial B_{1z}}{\partial \vartheta} - \frac{\partial B_{1\vartheta}}{\partial z}\right) - \frac{v_\perp^2 + 2v_\parallel^2}{2\omega_{c0} B_0 r}\left(h_z \frac{\partial \boldsymbol{h}\cdot\boldsymbol{B}_1}{\partial \vartheta} - h_\vartheta \frac{\partial \boldsymbol{h}\cdot\boldsymbol{B}_1}{\partial z}\right). \quad (23)$$

Expanding the perturbation field in a Fourier series,

$$\boldsymbol{B}_1 = \mathrm{Re}\sum_{\mathbf{m}} \boldsymbol{B}_{\mathbf{m}} \mathrm{e}^{\mathrm{i}m_\vartheta \vartheta + \mathrm{i}k_z z}, \qquad \Phi_1 = \mathrm{Re}\sum_{\mathbf{m}} \Phi_{\mathbf{m}} \mathrm{e}^{\mathrm{i}m_\vartheta \vartheta + \mathrm{i}k_z z}, \quad (24)$$

the radial drift velocity and the perturbed distribution function are expanded accordingly

$$v^r_{g1} = \mathrm{Re}\sum_{\mathbf{m}} v^r_{\mathbf{m}} \mathrm{e}^{\mathrm{i}m_\vartheta \vartheta + \mathrm{i}k_z z}, \quad \tilde{f} = \mathrm{Re}\sum_{\mathbf{m}} f_{\mathbf{m}} \mathrm{e}^{\mathrm{i}m_\vartheta \vartheta + \mathrm{i}k_z z}. \quad (25)$$

Denoting the projection to the flux surface of the perpendicular wave vector and parallel wave vector as

$$k_\perp = \frac{1}{r}\left(h_z m_\vartheta - h_\vartheta k_z\right), \qquad k_\parallel = h^\vartheta m_\vartheta + h^z k_z, \quad (26)$$

and introducing similar notation for the magnetic field components,

$$B_{\mathbf{m}\perp} = \frac{1}{r}\left(h_z B_{\mathbf{m}\vartheta} - h_\vartheta B_{\mathbf{m}z}\right) = \boldsymbol{B}_{\mathbf{m}} \times \boldsymbol{h}\cdot\nabla r, \quad (27)$$

$$B_{\mathbf{m}\parallel} = h^\vartheta B_{\mathbf{m}\vartheta} + h^z B_{\mathbf{m}z} = \boldsymbol{h}\cdot\boldsymbol{B}_{\mathbf{m}}, \quad (28)$$

the Fourier amplitude of the radial drift velocity is obtained as

$$v^r_{\mathbf{m}} = \frac{v_\parallel}{B_0} B^r_{\mathbf{m}} - \frac{\mathrm{i}ck_\perp}{B_0}\Phi_{\mathbf{m}} - \frac{\mathrm{i}k_\perp v_\perp^2}{2\omega_{c0} B_0} B_{\mathbf{m}\parallel} - \frac{\mathrm{i}k_\parallel v_\parallel^2}{\omega_{c0} B_0} B_{\mathbf{m}\perp}. \quad (29)$$

Respectively, the kinetic equation (21) for the Fourier amplitudes of the distribution function is

$$\hat{L} f_{\mathbf{m}} \equiv \mathrm{i}\left(k_\parallel v_\parallel + \omega_E\right) f_{\mathbf{m}} - \hat{L}_c f_{\mathbf{m}} = -\left(A_1 + \frac{m\left(v_\perp^2 + v_\parallel^2\right)}{2T} A_2\right) f_0\, v^r_{\mathbf{m}}, \quad (30)$$

where

$$\omega_E = k_\perp v_{E\perp} = \frac{ck_\perp}{B_0}\frac{\partial \Phi_0}{\partial r} \quad (31)$$

is the electric rotation frequency, and the fluxes (18) and (19) are

$$\Gamma = \frac{1}{2}\mathrm{Re}\sum_{\mathbf{m}}\int \mathrm{d}^3 p\; f_{\mathbf{m}}\, v^{r*}_{\mathbf{m}}, \quad (32)$$

$$Q = \frac{1}{2}\mathrm{Re}\sum_{\mathbf{m}}\int \mathrm{d}^3 p\; \frac{m\left(v_\perp^2 + v_\parallel^2\right)}{2} f_{\mathbf{m}}\, v^{r*}_{\mathbf{m}}. \quad (33)$$

In the collisionless case with $\hat{L}_c \to 0$, equation (30) is algebraic and the solution is

$$f_{\mathbf{m}} = \frac{\mathrm{i}v^r_{\mathbf{m}}}{k_\parallel v_\parallel + \omega_E - \mathrm{i}o}\left(A_1 + \frac{m\left(v_\perp^2 + v_\parallel^2\right)}{2T} A_2\right) f_0, \quad (34)$$

where the infinitesimal o denotes the Landau contour for the velocity space integration. Substituting this solution into fluxes (32) and (33), the fluxes can be expressed in the standard form

$$\Gamma = -n\left(D_{11}A_1 + D_{12}A_2\right), \qquad Q = -nT\left(D_{21}A_1 + D_{22}A_2\right), \quad (35)$$

where the elements of the transport coefficient matrix are

$$D_{kl} = \frac{\pi}{2n_0}\sum_{\mathbf{m}}\int \mathrm{d}^3 p\; \delta\left(k_\parallel v_\parallel + \omega_E\right)\left|v^r_{\mathbf{m}}\right|^2 a_k a_l f_0, \quad (36)$$

with $a_k = a_k(v_\perp, v_\parallel)$ given by

$$a_1 = 1, \qquad a_2 = \frac{m\left(v_\perp^2 + v_\parallel^2\right)}{2T}. \quad (37)$$

Integration over parallel momentum gives, in particular, for D_{11}

$$D_{11} = \frac{\sqrt{\pi}|Z|}{2|\omega_E|}\mathrm{e}^{-Z^2}\frac{1}{v_T^2} \times \int_0^\infty \mathrm{d}v_\perp v_\perp \exp\left(-\frac{v_\perp^2}{2v_T^2}\right)\left|v^r_{\mathbf{m}}\right|^2_{v_\parallel = -\omega_E/k_\parallel}, \quad Z = -\frac{\omega_E}{\sqrt{2}k_\parallel v_T}. \quad (38)$$

This result agrees with the result of the canonical Hamiltonian action-angle formalism following from equation (8) of [20]. In fact, the first three terms in (29), which describe parallel motion, $\boldsymbol{E}\times\boldsymbol{B}$ drift and gradient-B drift, correspond to the perturbed Hamiltonian in the first-order expansion of [6] and the last term (curvature drift) formally belongs to the next order. Ignoring this term and expressing the radial velocity through the resonant Hamiltonian,

$$v^r_{\mathbf{m}}\big|_{v_\parallel = -\omega_E/k_\parallel} = -\frac{\mathrm{i}ck_\perp}{eB_0} H_{\mathbf{m}}, \qquad H_{\mathbf{m}} = \frac{\mathrm{i}}{k_\parallel}\left(eE^{\mathrm{fl}}_{\mathbf{m}\parallel} - \frac{mv_\perp^2}{2B_0}\left(\boldsymbol{h}\cdot\nabla B\right)_{\mathbf{m}}\right) \quad (39)$$

one obtains the result of Hamiltonian theory, where the contribution of the first two terms in (29) has been combined in the Hamiltonian into the parallel electric field in the moving reference frame in which the equilibrium electric field vanishes (rest frame of the fluid), $E^{\mathrm{fl}}_{\mathbf{m}\parallel}$, and the gradient-$B$ drift results in the mirroring force. This form of the Hamiltonian shows that parallel streaming and $\boldsymbol{E}\times\boldsymbol{B}$ drift are linked to the usual Landau damping and the gradient-B drift is directly related to the TTMP-effect.

In the general collisional case, the solution of (30) is expressed through a Green's function,

$$f_{\mathbf{m}}(v_\parallel) = -\int_{-\infty}^{\infty}\mathrm{d}v'_\parallel\; G_{\mathbf{m}}(v_\parallel, v'_\parallel)\left(A_1 + a_2(v_\perp, v'_\parallel)A_2\right) \times f_0(v_\perp, v'_\parallel)\; v^r_{\mathbf{m}}(v_\perp, v'_\parallel), \quad (40)$$

which satisfies

$$\hat{L} G_{\mathbf{m}}(v_\parallel, v'_\parallel) = \delta(v_\parallel - v'_\parallel). \quad (41)$$

Without the integral term in the collision operator, this function was obtained in [7] for the linear collisional model of RMP shielding. Actually, it also describes the case with all cyclotron harmonics m_ϕ retained, in a time-varying field for a drifting Maxwellian if one replaces in operator $\hat{L}$, equation (30), the

electric rotation frequency ω_E with $\omega_E+m_\phi\omega_c+k_\parallel V_\parallel-\omega$, where $V_\parallel$ is the parallel fluid velocity of a given species and ω is the perturbation frequency. Substituting (40) into the fluxes (32) and (33), the transport coefficients in (35) become

$$D_{kl}=\frac{\pi m^3}{n}\mathrm{Re}\sum_{\mathbf{m}}\int_0^\infty \mathrm{d}v_\perp\, v_\perp\int_{-\infty}^\infty \mathrm{d}v_\parallel\int_{-\infty}^\infty \mathrm{d}v'_\parallel\, G_{\mathbf{m}}(v_\parallel,v'_\parallel)\times v^{r*}_{\mathbf{m}}(v_\perp,v_\parallel)v^r_{\mathbf{m}}(v_\perp,v'_\parallel)a_k(v_\perp,v_\parallel)a_l(v_\perp,v'_\parallel)f_0(v_\perp,v'_\parallel). \tag{42}$$

Since transport coefficients are obtained here for unperturbed flux surfaces, it should be checked that for the case of ideal MHD perturbations the transport vanishes in the absence of magnetic drifts. The condition of alignment of perturbed magnetic surfaces and equipotentials in linear order is

$$\boldsymbol{B}_0\cdot\boldsymbol{E}_1+\boldsymbol{B}_1\cdot\boldsymbol{E}_0=0. \tag{43}$$

In terms of Fourier amplitudes this condition becomes

$$-\mathrm{i}k_\parallel\Phi_{\mathbf{m}}B_0-\Phi'_0B^r_{\mathbf{m}}=E^{\mathrm{fl}}_{\mathbf{m}\parallel}=0,\qquad \Phi'_0\equiv\frac{\partial\Phi_0}{\partial r}. \tag{44}$$

Obviously, in the collisionless case the transport vanishes completely because the resonant Hamiltonian (39) is zero in the absence of a magnetic drift (TTMP term). With the help of (31) and (44), the first two terms in (29) can be presented as

$$v^r_{\mathbf{m}}=\frac{v_\parallel}{B_0}B^r_{\mathbf{m}}-\mathrm{i}\omega_E\frac{\Phi_{\mathbf{m}}}{\Phi'_0}=-\mathrm{i}\frac{\Phi_{\mathbf{m}}}{\Phi'_0}\left(k_\parallel v_\parallel+\omega_E\right). \tag{45}$$

Using the following properties of the collision operator,

$$\hat{L}_{\mathrm{cp}}f_0=0,\qquad \hat{L}_{\mathrm{cp}}v_\parallel^2f_0=0, \tag{46}$$

it can be checked that the solution of (30) with $v^r_{\mathbf{m}}$ in the form (45) is

$$f_{\mathbf{m}}=\left(A_1+\frac{m\left(v_\perp^2+v_\parallel^2\right)}{2T}A_2\right)f_0\frac{\Phi_{\mathbf{m}}}{\Phi'_0}. \tag{47}$$

Substituting this solution into (32) and (33), one gets $\Gamma=Q=0$ because the sub-integrands are purely imaginary. It should be noted that the second property (46) is provided by the integral part of the collision operator (4). The Ornstein–Uhlenbeck operator alone would result in fake heat fluxes for the case of ideal MHD.

It is useful to estimate the role of the various terms in (29). In the resonant layer, the perturbed equipotential surfaces do not repeat the perturbed magnetic surfaces anymore (see figures 6, 7, 8, 11). Therefore, the parallel streaming and the $\boldsymbol{E}\times\boldsymbol{B}$ drift do not balance each other and one can compare the last two terms describing the magnetic drift in (29) with the first term. From Maxwell equations one can estimate the relative scale of the various magnetic field components as follows:

$$B^r_{\mathbf{m}}\sim k_\perp\Delta r\,B_{\mathbf{m}\perp},\qquad B_{\mathbf{m}\parallel}\sim k_\parallel k_\perp^{-1}B_{\mathbf{m}\perp}, \tag{48}$$

where Δr is the typical radial width of the resonant layer. The second estimate (48) shows that actually the gradient-B drift (third term in (29)) is of the same order as the curvature drift (last term), which seems to be much smaller because of $k_\parallel\sim\Delta r k_\perp R^{-1}\ll k_\perp$. The parallel component of the perturbation magnetic field is the smallest and, therefore, is usually ignored in most MHD theories, which assume that the plasma is 'incompressible'. Comparing now the magnetic drifts with parallel streaming, one obtains that they provide a correction of the order of $k_\parallel\rho(k_\perp\Delta r)^{-1}\sim\rho R^{-1}\ll 1$, which can be safely ignored in the resonant layer. Of course, one cannot do this in the remaining ideal plasma where the magnetic drifts are the only source of cross-field transport caused by the (non-resonant) magnetic perturbations and where they are responsible for the neoclassical toroidal viscosity effect [18, 19]. This effect, however, is essentially dependent on the plasma toroidicity and cannot be adequately described in a straight cylinder geometry. Since the main interest here is in the effects of the resonant interaction localized in the resonant layer, magnetic drifts are ignored from now on.

Performing in (42) the integration over the perpendicular velocity, the transport coefficients are expressed through dimensionless moments of Green's function,

$$\begin{aligned}
D_{11}&=\frac{1}{2\nu B_0^2}\sum_{\mathbf{m}}(c^2|E_{\mathbf{m}\perp}|^2\mathrm{Re}(I^{00})+2cv_T\mathrm{Re}(E^*_{\mathbf{m}\perp}B^r_{\mathbf{m}})\\
&\quad\times\mathrm{Re}(I^{10})+v_T^2|B^r_{\mathbf{m}}|^2\mathrm{Re}(I^{11})),\\
D_{12}&=\frac{1}{2\nu B_0^2}\sum_{\mathbf{m}}(c^2|E_{\mathbf{m}\perp}|^2\mathrm{Re}(I^{00}+\tfrac{1}{2}I^{20})\\
&\quad+2cv_T\mathrm{Re}(E^*_{\mathbf{m}\perp}B^r_{\mathbf{m}})\mathrm{Re}(I^{10}+\tfrac{1}{4}I^{30}+\tfrac{1}{4}I^{21})\\
&\quad+v_T^2|B^r_{\mathbf{m}}|^2\mathrm{Re}(I^{11}+\tfrac{1}{2}I^{31}))=D_{21},\\
D_{22}&=\frac{1}{2\nu B_0^2}\sum_{\mathbf{m}}(c^2|E_{\mathbf{m}\perp}|^2\mathrm{Re}(2I^{00}+I^{20}+\tfrac{1}{4}I^{22})\\
&\quad+2cv_T\mathrm{Re}(E^*_{\mathbf{m}\perp}B^r_{\mathbf{m}})\mathrm{Re}(2I^{10}+\tfrac{1}{2}I^{30}+\tfrac{1}{2}I^{21}+\tfrac{1}{4}I^{32})\\
&\quad+v_T^2|B^r_{\mathbf{m}}|^2\mathrm{Re}(2I^{11}+I^{31}+\tfrac{1}{4}I^{33})),
\end{aligned} \tag{49}$$

defined by

$$I^{mn}(x_1,x_2)=\frac{\nu}{\sqrt{2\pi}v_T^{m+n+1}}\times\int_{-\infty}^\infty \mathrm{d}v_\parallel\int_{-\infty}^\infty \mathrm{d}v'_\parallel\, G_{\mathbf{m}}(v_\parallel,v'_\parallel)\exp\left(-\frac{v'^2_\parallel}{2v_T^2}\right)v_\parallel^m v'^n_\parallel. \tag{50}$$

Here, the dimensionless arguments are

$$x_1=\frac{k_\parallel v_T}{\nu},\qquad x_2=-\frac{\omega_E}{\nu}. \tag{51}$$

The transport coefficient matrix (49) is Onsager-symmetric due to the following property of the moments of energy-preserving Green's function [8]:

$$I^{21}-I^{30}=0. \tag{52}$$

The moments of the energy-preserving Green's function $G_{\mathbf{m}}$ can be expressed through the moments of Green's function for the pure Ornstein–Uhlenbeck collision model, $G^{\mathrm{D}}_{\mathbf{m}}$, i.e. the solution to

$$\mathrm{i}\left(k_\parallel v_\parallel+\omega_E\right)G^{\mathrm{D}}_{\mathbf{m}}(v_\parallel,v'_\parallel)-\hat{L}_{\mathrm{cD}}G^{\mathrm{D}}_{\mathbf{m}}(v_\parallel,v'_\parallel)=\delta(v_\parallel-v'_\parallel) \tag{53}$$

obtained in [7]. The relation between the two Green's functions is

$$G_{\mathbf{m}}(v_\parallel, v'_\parallel) = G^{\mathrm{D}}_{\mathbf{m}}(v_\parallel, v'_\parallel) + \frac{\nu C^{-1}_{\mathbf{m}}}{\sqrt{2\pi}\, v_T} \times \int_{-\infty}^{\infty} \mathrm{d}v'''_\parallel G^{\mathrm{D}}_{\mathbf{m}}(v_\parallel, v'''_\parallel) \exp\left(-\frac{v'''^2_\parallel}{2v_T^2}\right)\left(\frac{v'''^2_\parallel}{v_T^2} - 1\right) \times \int_{-\infty}^{\infty} \mathrm{d}v''_\parallel \left(\frac{v''^2_\parallel}{v_T^2} - 1\right) G^{\mathrm{D}}_{\mathbf{m}}(v''_\parallel, v'_\parallel), \tag{54}$$

where the constant $C_{\mathbf{m}}$ is

$$C_{\mathbf{m}} = 1 - \frac{\nu}{\sqrt{2\pi}\, v_T} \int_{-\infty}^{\infty} \mathrm{d}v''_\parallel \left(\frac{v''^2_\parallel}{v_T^2} - 1\right) \times \int_{-\infty}^{\infty} \mathrm{d}v'_\parallel G^{\mathrm{D}}_{\mathbf{m}}(v''_\parallel, v'_\parallel) \exp\left(-\frac{v'^2_\parallel}{2v_T^2}\right)\left(\frac{v'^2_\parallel}{v_T^2} - 1\right). \tag{55}$$

This relation can be checked by direct substitution into (41). The corresponding relation between the moments is

$$I^{nm} = I^{mn}_{\mathrm{D}} + \frac{\left(I^{m0}_{\mathrm{D}} - I^{m2}_{\mathrm{D}}\right)\left(I^{n0}_{\mathrm{D}} - I^{n2}_{\mathrm{D}}\right)}{1 - I^{00}_{\mathrm{D}} + 2I^{20}_{\mathrm{D}} - I^{22}_{\mathrm{D}}}, \tag{56}$$

with I^{mn}_{D} given by (50), where $G_{\mathbf{m}}$ is replaced by $G^{\mathrm{D}}_{\mathbf{m}}$. The dimensionless moments I^{mn}_{D} are related to the dimensional moments (47) of [20] as follows:

$$I^{mn}_{\mathrm{D}} = \frac{\nu}{\sqrt{2\pi}\, v_T^{m+n+1}} W^{mn}_0, \tag{57}$$

and can be explicitly written as

$$I^{mn}_{\mathrm{D}}(x_1, x_2) = \left\{ \frac{\partial^{m+n}}{\partial\alpha^m \partial\beta^n} \int_0^\infty \mathrm{d}\tau \exp\left[\left(\mathrm{i}x_2 - x_1^2\right)\tau \right.\right. \tag{58}$$

$$\left.\left. + \left(\alpha + \mathrm{i}x_1\right)\left(\beta + \mathrm{i}x_1\right)\left(\mathrm{e}^{-\tau} - 1\right) + \frac{(\alpha+\beta)^2}{2} \right] \right\}_{\alpha,\beta=0}. \tag{59}$$

Finally, one can express the Fourier amplitude of the parallel linear response current density through the thermodynamic forces (22) and the moments of Green's function,

$$j_{\mathbf{m}\parallel} = e \int \mathrm{d}^3 p\; v_\parallel f_{\mathbf{m}} \tag{60}$$

$$= -\frac{nev_T}{\nu B_0}\left(\left(\left(A_1 + A_2\right) I^{10} + \frac{1}{2} A_2 I^{21} \right) cE_{\mathbf{m}\perp} + \left(\left(A_1 + A_2\right) I^{11} + \frac{1}{2} A_2 I^{31} \right) v_T B^r_{\mathbf{m}} \right).$$

This expression where only the gyroaveraged part of the distribution function is taken into account agrees well with the full kinetic expression used for the solution of Maxwell equations. It is fully analogous to the expression for the parallel flow in the neoclassical theory and, respectively, the current summed over the species is analogous to the bootstrap current in toroidal devices.

2.2. Linear response model

The calculation of the transport coefficients obtained in the previous subsection requires the knowledge of the perturbation field, which is obtained from the solution of the linear problem. As in [6, 7, 11] this problem is solved for the straight cylinder tokamak model. In this model, Maxwell equations,

$$\nabla \times \tilde{\boldsymbol{E}} = \frac{\mathrm{i}\omega}{c}\tilde{\boldsymbol{B}}, \qquad \nabla \times \tilde{\boldsymbol{B}} = -\frac{\mathrm{i}\omega}{c}\tilde{\boldsymbol{E}} + \frac{4\pi}{c}\tilde{\boldsymbol{j}}, \tag{61}$$

are solved in cylindrical geometry retaining the Maxwell current and using a plasma response current $\tilde{\boldsymbol{j}}$ given by kinetic theory. In contrast to the quasilinear transport equations derived from the gyrokinetic equation in the previous section, the linear conductivity operator is obtained from the full kinetic equation. It takes into account gyromotion and polarization currents (in case of time varying fields), and, therefore, the linear model covers all types of plasma oscillations. For example, resistive wall modes have been computed with this model recently [21]. For a single spatial harmonic of the perturbation field, $\tilde{E}_i$, $\tilde{j}^i \propto \exp(\mathrm{i}m_\vartheta \vartheta + \mathrm{i}k_z z)$, the contravariant components of the perturbed current density $\tilde{\boldsymbol{j}}$ are linked to the co-variant components of the perturbation electric field $\tilde{\boldsymbol{E}}$ by a differential conductivity operator in the form

$$\tilde{j}^k(r, \vartheta, z) = \frac{1}{r}\sum_{n,n'=0}^{N} (-1)^n \frac{\partial^n}{\partial r^n}\left(r\, \sigma^{kl}_{(n,n')}(r, \boldsymbol{k}) \frac{\partial^{n'}}{\partial r^{n'}} \tilde{E}_l(r, \vartheta, z) \right), \tag{62}$$

where the derivatives result from the finite Larmor radius (FLR) expansion of the exact integral conductivity operator. The elements of the conductivity operator $\sigma^{kl}_{(n,n')}$ introduced in [6] were first obtained for the collisionless model and the Krook collision model was used for crude estimates of collisional effects. Later on, they were upgraded in [7] where a Fokker–Planck type Ornstein–Uhlenbeck operator was used for the collisions and a more compact FLR expansion was introduced. In this study, the collision model is upgraded again to include energy conservation as described in the previous subsection. This upgrade, nevertheless, does not affect the formulae connecting the moments of Green's function, I^{mn}, with the elements of the conductivity operator $\sigma^{kl}_{(n,n')}$. Therefore, the reader is forwarded to [7] for details of the conductivity operator.

Up to the now a special FLR expansion has been used that ensures Galilean invariance of the resonant part of the plasma response current. In this expansion summations over n and n' in (62) are limited by $N - 1$ if the relevant coordinate index (k or j, respectively) corresponds to the radial variable. In the case of high expansion orders, $N > 1$, such conductivity operators lead to very short scale fake modes (scales below electron Larmor radius), which are absent in the final solution but make the problem numerically very stiff. In this paper, a different expansion, denoted with $N++$, is introduced for $N > 1$. In this expansion, the selection rule is reversed, i.e. the summations over radial components are extended to $N+1$. Such expansions are not automatically Galilean invariant but are much more stable numerically because the smallest scale of fake modes is limited by the ion Larmor radius scale. Since the violation of the Galilean invariance scales with terms ignored in the FLR expansion, it should be small for high N if the expansion order is sufficient. Here, such an expansion of the order 3++ where the largest terms ignored are of the fourth order in Larmor radius is used to verify the standard $N = 1$ expansion used in all computations.

2.3. Balance equations

The reaction of the equilibrium plasma parameter profiles on the RMP is modelled with the help of the following set of balance equations in the standard form for general toroidal geometry:

$$\frac{\partial n_\mathrm{e}}{\partial t} + \frac{1}{S}\frac{\partial}{\partial r} S\left(\Gamma^{(\mathrm{EM})}_{(\mathrm{e})} + \Gamma^{(\mathrm{A})}_{(\mathrm{e})}\right) = S^{(0)}_n, \tag{63}$$

$$\frac{\partial}{\partial t} m_\mathrm{i} n_\mathrm{i} \langle g_{\varphi\varphi}\rangle V^\varphi_\mathrm{i} - \frac{1}{S}\frac{\partial}{\partial r} S m_\mathrm{i} n_\mathrm{i} \langle g_{\varphi\varphi}\rangle \mu^{(\mathrm{A})}_\varphi \frac{\partial V^\varphi_\mathrm{i}}{\partial r} = T^{(\mathrm{EM})}_{\varphi(\mathrm{e})} + T^{(\mathrm{EM})}_{\varphi(i)} + T^{(0)}_\varphi, \tag{64}$$

$$\frac{\partial}{\partial t}\frac{3}{2} n_\mathrm{e} T_\mathrm{e} + \frac{1}{S}\frac{\partial}{\partial r} S\left(Q^{(\mathrm{EM})}_{(\mathrm{e})} + Q^{(\mathrm{A})}_{(\mathrm{e})}\right) = e_\mathrm{e}\frac{\partial \Phi_0}{\partial r}\Gamma^{(\mathrm{EM})}_{(\mathrm{e})} + S^{(0)}_{w(\mathrm{e})}, \tag{65}$$

$$\frac{\partial}{\partial t}\frac{3}{2} n_\mathrm{i} T_\mathrm{i} + \frac{1}{S}\frac{\partial}{\partial r} S\left(Q^{(\mathrm{EM})}_{(\mathrm{i})} + Q^{(\mathrm{A})}_{(\mathrm{i})} + Q^{(\mathrm{NEO})}_{(\mathrm{i})}\right) = e_\mathrm{i}\frac{\partial \Phi_0}{\partial r}\Gamma^{(\mathrm{EM})}_{(\mathrm{i})} + S^{(0)}_{w(\mathrm{i})}, \tag{66}$$

which describe the evolution of the plasma density n_e (electron continuity equation (63)), the flux surface averaged ion toroidal rotation frequency V^φ_i (toroidal momentum balance equation (64)), the electron, T_e, and the ion, T_i, temperatures (heat balance equations (65) and (66) respectively). Here, r, S and $\langle g_{\varphi\varphi}\rangle \sim R^2$ are the effective radius [22], the flux surface area and the flux surface averaged co-variant toroidal component of the symmetry flux coordinates metric tensor, respectively.

Electron and ion particle and heat fluxes driven by the perturbation field, $\Gamma^{(\mathrm{EM})}_{(\mathrm{e,i})}$ and $Q^{(\mathrm{EM})}_{(\mathrm{e,i})}$, respectively, are given by equations (35) and (49) of section 2.1, and the respective toroidal torque densities $T^{(\mathrm{EM})}_{\varphi(\mathrm{e,i})}$ are determined by particle fluxes through the flux–force relation [23],

$$T^{(\mathrm{EM})}_{\varphi(\mathrm{e,i})} = -\frac{e_\mathrm{e,i}}{c}\sqrt{g}B^\vartheta_0\Gamma^{(\mathrm{EM})}_{(\mathrm{e,i})}, \tag{67}$$

where $\sqrt{g}$ and B^ϑ_0 are the metric determinant and the contra-variant poloidal component of the equilibrium magnetic field, respectively.

The anomalous particle and heat fluxes, $\Gamma^{(\mathrm{A})}_{(\mathrm{e,i})}$ and $Q^{(\mathrm{A})}_{(\mathrm{e,i})}$, respectively, are given by the simple model used in [11] where

$$\Gamma^{(\mathrm{A})}_{(\mathrm{e,i})} = -D_\perp\frac{\partial n_\mathrm{e,i}}{\partial r}, \qquad Q^{(\mathrm{A})}_{(\mathrm{e,i})} = -\frac{3}{2}D_\perp\frac{\partial n_\mathrm{e,i}T_\mathrm{e,i}}{\partial r}. \tag{68}$$

This model results from the assumption that turbulence leads in the reference frame where the equilibrium radial electric field is zero to diffusive particle motion with diffusion coefficient $D_\perp$ independent of particle velocity. In this frame, particle and heat fluxes can be, again, computed with the help of (35) and taking into account that $D_{11} = D_\perp$, $D_{12} = D_{21} = (3/2)D_\perp$ and $D_{22} = (15/4)D_\perp$. Consequently, the anomalous shear viscosity coefficient $\mu^{(\mathrm{A})}_\varphi$ describing the radial diffusion of the ion toroidal momentum is equal to $D_\perp$ too, and the electron viscosity, which is $m_\mathrm{e}/m_\mathrm{i}$ times smaller than ion viscosity, is ignored. The above anomalous transport model leads to ambipolar transport and, consequently, gives no overall torque in (64), and also produces no turbulent heating (no terms with electric field on the right-hand sides of (65) and (66)).

The only neoclassical flux taken into account is the ion heat flux, which is obtained by taking the low-collisionality limit of equation (6.131) of [24]:

$$Q^{(\mathrm{NEO})}_{(\mathrm{i})} = -1.32 n_\mathrm{i}\left(\frac{R}{r}\right)^{3/2}\frac{q^2 v^2_{T_\mathrm{i}}}{\omega^2_{\mathrm{ci}}\tau_\mathrm{i}}\frac{\partial T_\mathrm{i}}{\partial r}, \quad \tau_\mathrm{i} = \frac{3 m_\mathrm{i}^{1/2} T_\mathrm{i}^{3/2}}{4\pi^{1/2} e_\mathrm{i}^4 n_\mathrm{i}\Lambda}, \tag{69}$$

where Λ is the Coulomb logarithm.

The equilibrium radial electric field, which enters the thermodynamic forces (22) and the right-hand sides of (65) and (66), is determined from the condition on the poloidal ion velocity, which is set to the equilibrium neoclassical velocity (see, e.g., [25]):

$$V^\vartheta_\mathrm{i} = \frac{ckB_{0\varphi}}{e\sqrt{g}\langle B^2_0\rangle}\frac{\partial T_\mathrm{i}}{\partial r}, \tag{70}$$

where $B_{0\varphi}$ is the co-variant toroidal component of the equilibrium magnetic field, and the coefficient k is computed by the NEO-2 code [26]. Actually, this coefficient changes sign at the plasma edge in ASDEX Upgrade discharges considered here. The resulting electric field is

$$-\frac{\partial \Phi_0}{\partial r} = \frac{\sqrt{g}B^\vartheta_0}{c}\left(V^\varphi_\mathrm{i} - qV^\vartheta_i\right) + \frac{1}{e_\mathrm{i} n_\mathrm{i}}\frac{\partial n_\mathrm{i} T_\mathrm{i}}{\partial r}. \tag{71}$$

Finally, particle and energy sources $S^{(0)}_n$ and $S^{(0)}_{w(\mathrm{e,i})}$, respectively and the equilibrium torque density $T^{(0)}_\varphi$ are chosen in such a way [14, 27] that in the absence of the perturbation field, the balance equations result in a steady state for the experimental profiles of density, rotation frequency and temperatures, which are the input for the model.

2.4. Relation to real geometry

The quasilinear transport coefficients (49) are determined by the RMP electromagnetic field in the vicinity of the resonant surface. The estimate of this field for real tokamak geometry is obtained using the method similar to the one used in [11, 28]. Presenting the total tokamak field as a sum of the axisymmetric equilibrium field and the perturbation field, $\boldsymbol{B} = \boldsymbol{B}_0 + \boldsymbol{B}_1$, these fields are expressed through vector potentials in symmetry flux coordinates $(\psi_\mathrm{tor}, \vartheta, \varphi)$ as follows:

$$\begin{aligned}\boldsymbol{B}_0 &= \nabla\psi_\mathrm{pol}\times\nabla\varphi + B_{0\varphi}\nabla\varphi,\\ \boldsymbol{B}_1 &= \nabla A_{1\psi}\times\nabla\psi_\mathrm{tor} + \nabla A_{1\vartheta}\times\nabla\vartheta.\end{aligned} \tag{72}$$

Here, ψ_tor and ψ_pol are the toroidal and poloidal magnetic fluxes (divided by 2π) of the axisymmetric magnetic field $\boldsymbol{B}_0$ given by the equilibrium code. Expanding the component $A_{1\vartheta}$ of the perturbation vector potential (the only one which determines the topology of the magnetic field and quasilinear effects in the resonant layer) in a Fourier series over the angles,

$$A_{1\vartheta} = 2\,\mathrm{Re}\sum_{n=1}^{\infty}\sum_{m=-\infty}^{\infty} A_{\vartheta;m,n}(\psi_\mathrm{tor})\,\mathrm{e}^{\mathrm{i}m\vartheta+\mathrm{i}n\varphi}, \tag{73}$$

the vacuum Fourier amplitudes, $A^{(\mathrm{vac})}_{\vartheta;m,n}$, computed from the perturbation field determined by the coil currents through the

Biot–Savart law, are replaced with shielded amplitudes

$$A_{\vartheta;m,n}(\psi_{\rm tor}) = A^{\rm (vac)}_{\vartheta;m,n}(\psi_{\rm tor}) T_{m,n}(\psi_{\rm tor}), \qquad (74)$$

where the form factors $T_{m,n}$ are defined through solutions of Maxwell equations for the cylinder geometry in plasma and in vacuum as

$$T_{m,n}(\psi_{\rm tor}) = \frac{B^{r\,\rm (plas)}_{\mathbf{m}}(r)}{B^{r\,\rm (vac)}_{\mathbf{m}}(r)}. \qquad (75)$$

Here, the effective radius r corresponds to the flux surface labelled by $\psi_{\rm tor}$. (It should be noted that these form factors do not tend to a constant value at the inner flux surfaces outside the resonant layer because $B^{r\,\rm (plas)}_{\mathbf{m}}(r)$ still satisfies there the ideal MHD equation of [29], see [6].) This method has been used in [11, 28] and is used here for estimation of the shielding effect on the perturbed magnetic field topology. Conversely, the transport coefficients (49) computed for the separate perturbation field modes $\mathbf{m}$ for the straight cylinder model are multiplied upon the summation with spectral weights given by

$$W_{\mathbf{m}} = \left| \frac{k_z A^{\rm (vac)}_{\vartheta;m,n}}{r B^{r\,\rm (vac)}_{\mathbf{m}}} \right|^2, \qquad (76)$$

and the relation between k_z and n is discussed at the beginning of this section. Thus, the problem of RMP field penetration and evolution of background parameters under the action of this field is fully determined. The problem is solved self-consistently tracing stepwise the time evolution of the background parameters with the help of the balance code solving equations (63)–(66) and updating the electromagnetic field at each time step with the help of the Maxwell equation solver KILCA [7].

Of course, the combination of the cylindrical plasma response model with realistic vacuum field computations presented here can be used for a qualitative analysis only. Since the linear model and the quasilinear model completely ignore mode coupling, which becomes strong near the separatrix where the metric tensor of flux coordinates is singular, quantitative results at the very plasma edge can be strongly affected by errors stemming from this simplification. In addition to this, the magnetic drift has been fully ignored in the quasilinear transport fluxes. As estimated for the cylindrical model in section 2.1, the effect of the magnetic drift is small in the narrow resonant layer being of interest here. At the same time, the effect of this drift (in particular, NTV viscosity) is the only one remaining in the bulk plasma where the perturbation field is described well by the ideal MHD equations. This effect, however, cannot be treated properly within the cylindrical model because it is mainly determined by toroidally trapped particles which are absent in the straight cylinder.

As shown in [30], non-axisymmetric neoclassical transport driven by the magnetic drift of trapped particle strongly increases near the island chain (at distances from the island chain which are larger than the island width, the bounce-averaged radial drift velocity scales inversely with this distance), and one may expect that it dominates in the resonant layer. However, this is not the case. The increase in the bounce-averaged velocity near the islands discussed in [30] is the result of the toroidal banana precession (weakly affected by the non-axisymmetric field) which gains the normal component across the perturbed flux surfaces due to the non-axisymmetric deformation of these surfaces. In the ideal plasma where the equipotential surfaces are aligned with the perturbed flux surfaces, the magnetic drift is the only mechanism for the transport across the magnetic surfaces. In the resistive layer, the mismatch between the equipotentials and the perturbed flux surfaces is of the order one. For simplicity, one can get such a mismatch assuming the equipotentials to be unperturbed. In such an example the $\boldsymbol{E} \times \boldsymbol{B}$ drift results in the usual, axisymmetric toroidal banana precession due to the electric field. This is typically faster than the precession due to the magnetic drift. Moreover, toroidal particle trapping does not play such an important role in the resonant layer as it plays at normal, strongly non-resonant flux surfaces where it prevents particle decorrelation from the perturbation field by parallel motion. Due to the proximity of field lines to the rational field line in the resonant layer, passing particles which are dominating in the transport stay in correlation with the perturbation field over a large number of poloidal turns, and their decorrelation occurs due to mechanisms already taken into account in the cylindrical model of this paper.

It should also be noted that the magnetic drift in the ideal plasma cannot be completely ruled out by the arguments above. The inverse scaling of the bounce-averaged magnetic drift velocity with distance from the island chain is not a general property of RMPs. Here it follows from the assumption that the radial component of the perturbation field changes weakly within the resonant layer and in its close proximity ('constant-ψ approximation'). If RMPs are shielded, this component often increases with distance (see, e.g., the form factors in figures 2–4), and the 'ideal' non-axisymmetric transport near the islands may contribute significantly. This should be taken into account in more accurate future models.

3. Application to ASDEX Upgrade shots and comparison with DIII-D

The linear model has been essentially upgraded since the publication of [11]. Therefore, the same DIII-D shot with the same parameters used in [11] as well as with the toroidal rotation velocity corrected in [13] is revisited and compared with ASDEX Upgrade discharges. The plasma density and temperatures for ASDEX Upgrade shot 26201 and for DIII-D shot 126006 are shown in figure 1. Formfactors (75) for DIII-D are shown in figure 2. For brevity, the notation for wave numbers in the figures is changed to the standard one, $m = m_\vartheta$ and $n = m_\varphi$. The revised formfactors for DIII-D are almost identical with results in [11] for modes in the core plasma where the shielding is essentially collisionless. However, they are modified for a few modes at the very edge where the Krook model overestimates the shielding roughly by a factor 5. Nevertheless, shielding at the edge stays strong and is sufficient in order to eliminate the ergodic layer in the pedestal, as already concluded in [11]. The formfactors for the updated toroidal velocity profile show that the resonance of total perpendicular electron fluid velocity $V_{\perp \rm e} = 0$ moved closer to the edge, actually to the pedestal top, and modes in the pedestal, except for the mode $m = -10$ that is near the equilibrium electric field reversal point (effects of this point are discussed in more detail

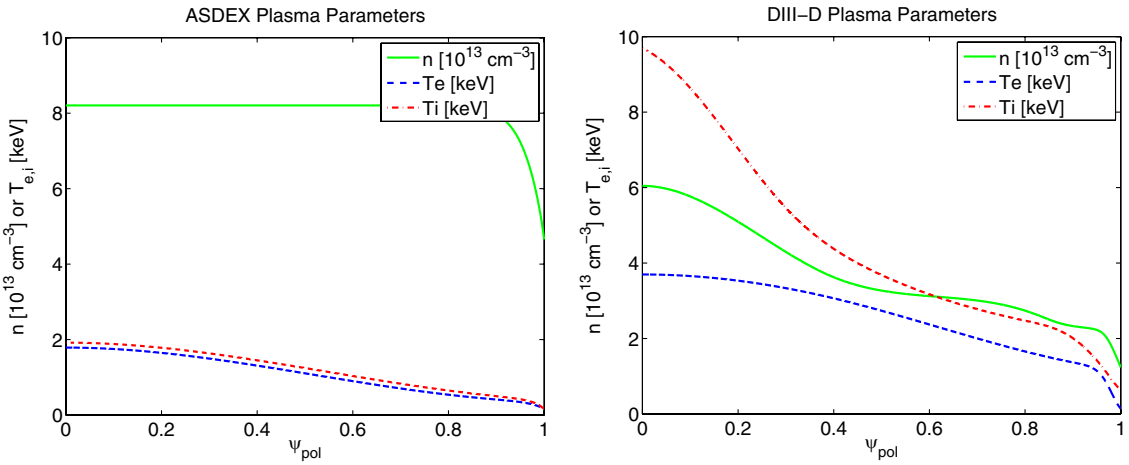

Figure 1. Plasma parameters versus the normalized poloidal flux for ASDEX Upgrade and DIII-D.

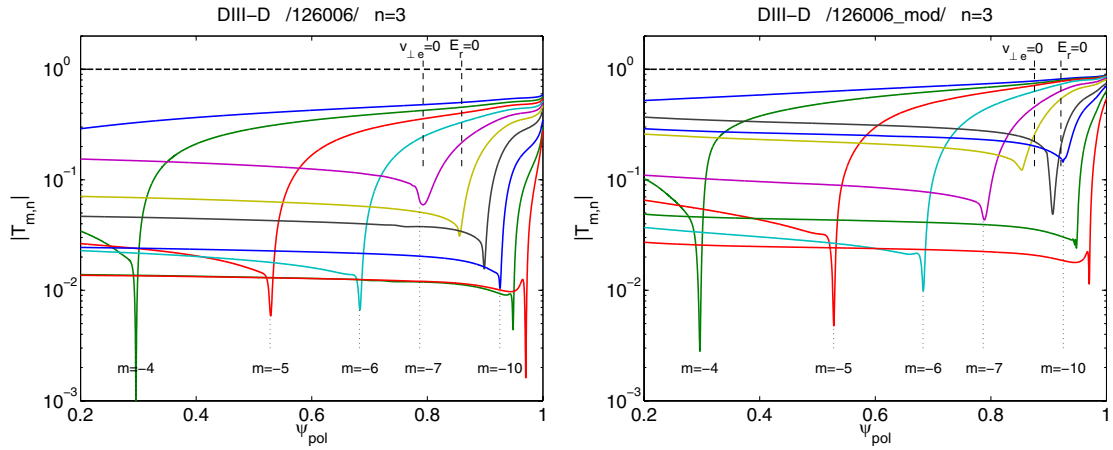

Figure 2. Formfactor modules versus the normalized poloidal flux for the main toroidal mode, $n = 3$, and various poloidal modes for DIII-D shot 126006 (left) and the same shot with updated toroidal velocity V_z (right) corresponding to figure 1 of [13]. Positions of fluid resonances $V_{\perp e} = 0$ and $E_r = 0$ are shown with dashed vertical lines.

in section 4), are again shielded by two orders of magnitude, which prevents the formation of an ergodic layer.

These results are in good agreement with results from the two-fluid MHD theory recently used to analyse the same DIII-D shot [9]. Such an agreement has already been observed earlier in [11] where the results were compared with [31] and certain agreement was achieved even in cases where MHD theory is far beyond its applicability range because the width of the resistive layer is orders of magnitude smaller than the ion Larmor radius (in the case of [9] it is five times smaller). This agreement can be understood as follows. For the parallel electron current density, which is more important than the parallel ion current density and primarily responsible for the RMP shielding, FLR effects are never important, even for collisionless resonant layers, which can be shown to be always wider than the electron Larmor radius. Therefore, the parallel current density (60) computed within the gyrokinetic theory and provided with the same electromagnetic field agrees with full kinetic theory employed in the KILCA code within a per cent of accuracy. This is, of course, not true for the perpendicular current density components, for that only qualitative agreement should be expected with MHD theory.

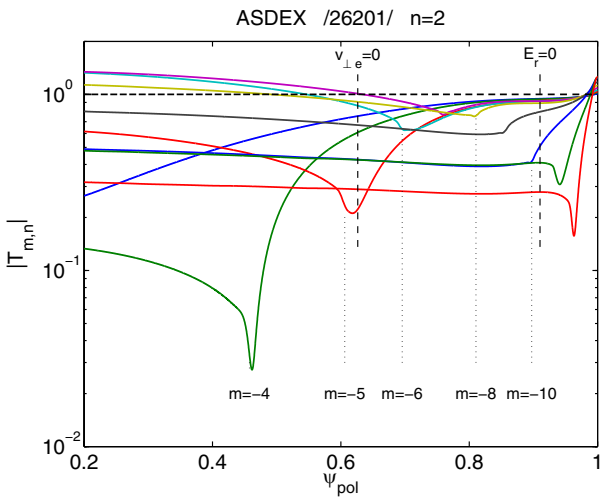

Figure 3. The same as in figure 2 for the main toroidal mode $n = 2$ for ASDEX Upgrade shot 26201.

The form factors for three ASDEX Upgrade discharges are shown in figures 3 and 4. Generally, the shielding is significantly (by an order of magnitude) smaller than in DIII-D and the shielding factor is about 10 or less. It can be seen

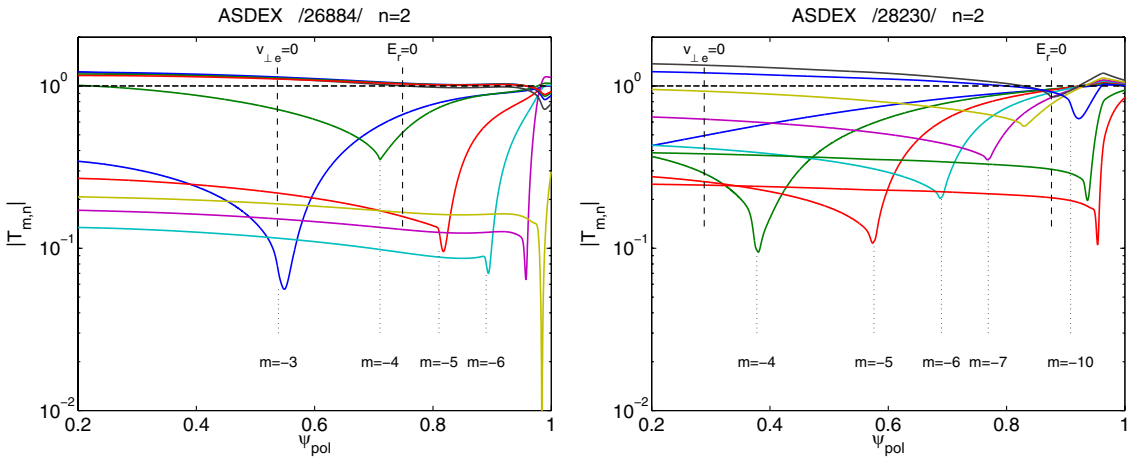

Figure 4. The same as in figure 3 for ASDEX Upgrade shot 26884 (left) and shot 28230 (right).

that for shot 26201 there is a rather broad region where the shielding is practically absent. In this region, the total electron fluid velocity $V_{\perp e}$ is rather small, although it is not zero and rather forms a plateau there (see figure 6).

Note that maximal penetration of the perturbation field is not necessarily reached at the point $V_{\perp e} = 0$ but is generally shifted from this velocity value with a shift proportional to the electron temperature gradient [6, 20]. The proportionality coefficient depends on plasma collisionality. The origin of this shift is evident from the gyrokinetic expression for the parallel current density (60) responsible for the shielding. The relative temperature gradient enters this expression through both thermodynamic forces in contrast to the relative density gradient, which enters through A_1 only. Thus, in the shielding current, these gradients generally cannot be combined into a sole pressure gradient term. A simple formula for this shift can be obtained in the collisionless limit, $x_2 \gg 1$ (see (51)), assuming a small change of $B^r_{\mathbf{m}}$ and $E_{\mathbf{m}\perp}$ in the resonant layer—the so-called 'constant psi' approximation, where shielding is due to the change in the $B^r_{\mathbf{m}}$ derivative within the layer. This change is proportional to the total parallel current in the layer given by the integral of (60) over radius, which in 'constant psi' approximation is reduced to an integration of the moments I^{mn} over x_1. For I^{10} and I^{21} these integrals give zero, while the integral of I^{31} is twice the integral of I^{11}. Thus, the total electron current is proportional to $\partial \ln(n_e T_e)/\partial r + e\partial\Phi_0/(T_e \partial r) - 0.5\partial \ln T_e/\partial r$, and the shielding is lost if the $\boldsymbol{E} \times \boldsymbol{B}$ velocity balances half of the diamagnetic velocity but not the whole one (the density gradient is practically absent there, see figure 1). This condition on gradients is the same as the condition for the reversal of quasilinear radial particle flux in the relevant regime [20]. Such a dependence of the parallel current on the gradients is similar to the dependence of parallel flow in the plateau regime [25] (coefficient $k = 0.5$ in (70)), which is the linear collisionless regime of neoclassical transport. Since the regime for the present cases is far from being collisionless (and even in the collisionless regime the constant-psi approximation does not apply, see the form factors in DIII-D core, figure 2) the shift coefficient is less than 1/2, but appears to be still sufficient to cause a loss of shielding in a wide region.

Form factors for shots 26884 and 28230 (figure 4) show the presence of unshielded modes too. However, these modes

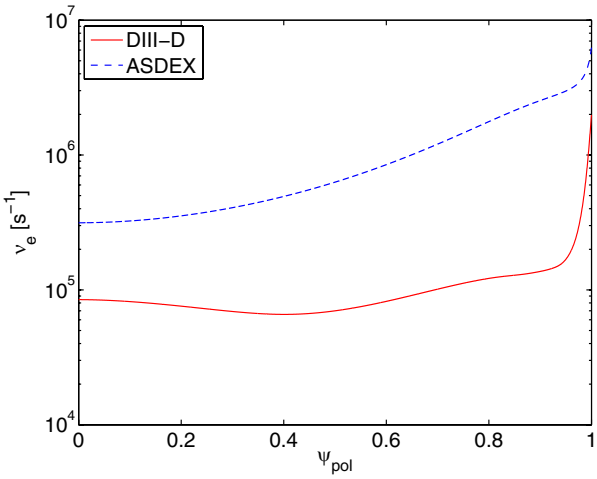

Figure 5. Electron collision frequencies in ASDEX Upgrade and DIII-D.

cannot be associated with electron fluid velocity resonance $V_{\perp e} = 0$ but rather with an equilibrium electric field reversal point $\Phi_0' = 0$, see figures 7 and 8. The reason for such an order of magnitude weaker shielding in ASDEX Upgrade when compared with the DIII-D shot 126006 is the one order of magnitude higher collisionality, see figure 5. The result of such weak shielding is that the ergodic magnetic field regions are not eliminated from the pedestal region (see the Poincaré plots in figures 6–8). They roughly cover the pedestal in shot 26201, go deeper into the core in shot 26884 and occupy lower half of the pedestal in shot 28230. Such a behaviour of shielded ergodic layers is a consequence of their behaviour in the vacuum case and this behaviour correlates well with the experimentally observed effect of the RMP coils on the ELMs and plasma performance. In particular, in shot 28230, where ergodic layer is the smallest in size and does not cover the whole pedestal region, no significant effect of RMP coils on ELMs and the plasma is observed, in shot 26201 ELMs are mitigated, and in shot 28230, where due to low q values the main perturbation modes are resonant at the edge and produce the widest ergodic layer, together with ELM mitigation a degradation of the electron temperature is observed. Such a

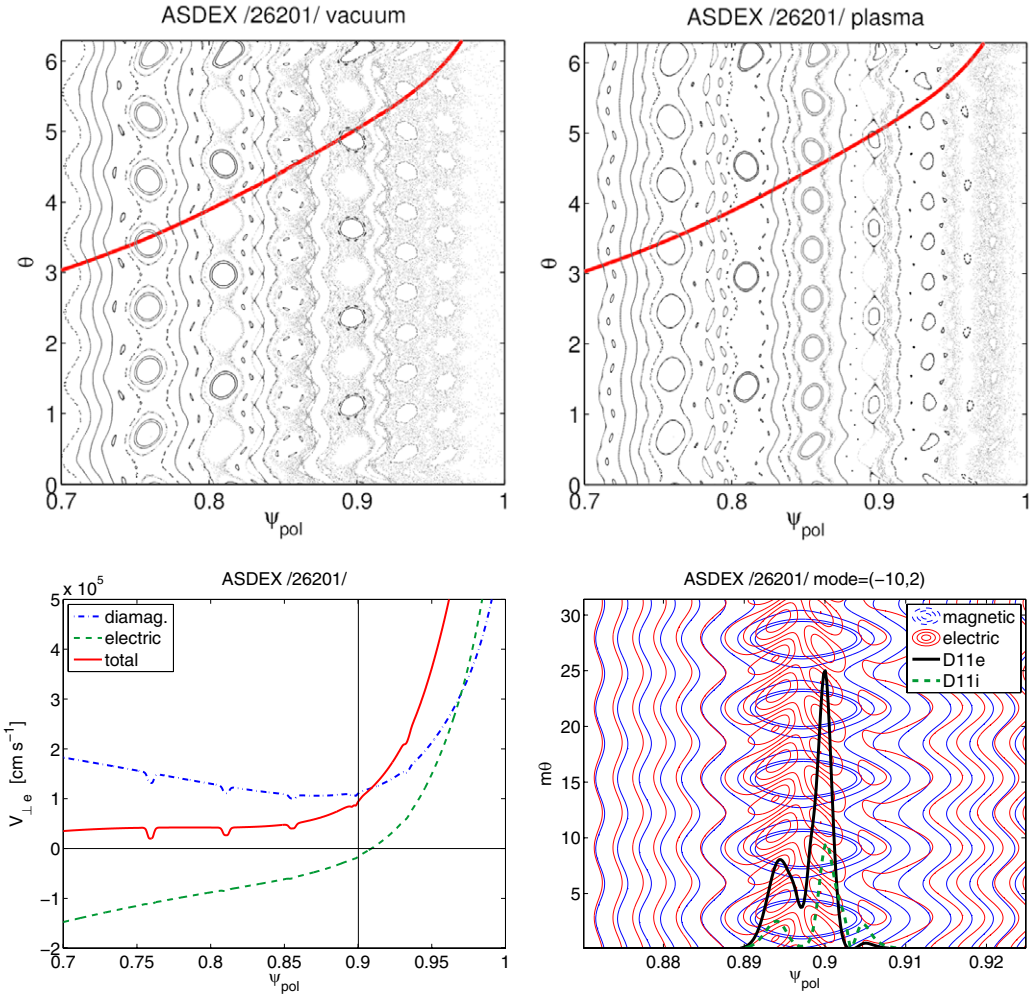

Figure 6. ASDEX Upgrade shot 26201. Upper panel: Poincaré plots of vacuum magnetic field (left) and with shielding taken into account. The solid curve shows the safety factor versus the normalized poloidal flux. Lower panel, left: total perpendicular electron fluid velocity (solid), diamagnetic electron velocity (dotted–dashed) and $\boldsymbol{E} \times \boldsymbol{B}$ velocity (dashed). The position of the resonance for the mode $(m, n) = (-10, 2)$ is shown by a vertical line. Lower panel, right: perturbed magnetic flux surfaces (blue) and equipotential surfaces (red) for the mode (−10,2). Thick solid and dashed curves show the electron and ion diffusion coefficient D_{11} versus the normalized poloidal flux.

degradation should be expected due to the enhanced parallel electron heat transport in the ergodic field [10, 32].

It should be noted that besides ASDEX Upgrade shots shown here, one more shot, shot 26196, was modelled. In this shot, the plasma parameters before switching on the RMP coils were the same as in shot 26201 but the coil polarity was odd instead of even. In this case, almost all main coil modes were resonant at the edge, and the resulting shielded ergodic layer was even wider than that in shot 26884. Nevertheless, a strong degradation of the plasma temperature was not reported for shot 26196. A possible reason is that the electron temperature at the edge was by a factor two lower in this shot than in shot 26884 and the plasma density was higher so that the parallel electron heat conductivity coefficient was almost an order of magnitude smaller in shot 26196 than in shot 26884. Therefore, the wide ergodic layer did not result in a strong electron heat transport.

For quasilinear modelling the following profile for the anomalous diffusion coefficient was assumed in (68):

$$D_\perp(r) = D_{\perp 0}\left(1 - 0.8\left(\frac{r}{a}\right)^3\right), \qquad (77)$$

where a is the effective radius of the separatrix and $D_0 = 10^4\,\mathrm{cm}^2\,\mathrm{s}^{-1}$. The steady-state diamagnetic, $\boldsymbol{E} \times \boldsymbol{B}$ drift and the total electron fluid velocity $V_{\perp e}$ obtained as a result of the quasilinear evolution are shown in the lower panels of figures 6–8. It can be seen that these velocities are strongly affected only in shot 28230 where the main coil modes with large amplitudes are resonant at the edge. The general trend of the quasilinear evolution is to eliminate the total velocity $V_{\perp e}$, and this occurs not so much due to the change in the rotation, but mainly due to the change in the electron temperature profile (plateau formation). Similar trends have been observed in quasilinear modelling within MHD theory in [14]. The formation of the plateau on the electron temperature does not necessarily lead to a flattening of the density profile where, sometimes, the gradient can become even steeper. This can be understood as follows. Assuming for simplicity that quasilinear transport coefficients are much larger in the resonant layer than the anomalous, the steady-state equilibrium is approximately given by $\Gamma_{(e)}^{(EM)} = 0$ and $Q_{(e)}^{(EM)} = 0$ with fluxes given by (35). Since in the presence of collisions the transport coefficient matrix is not degenerate,

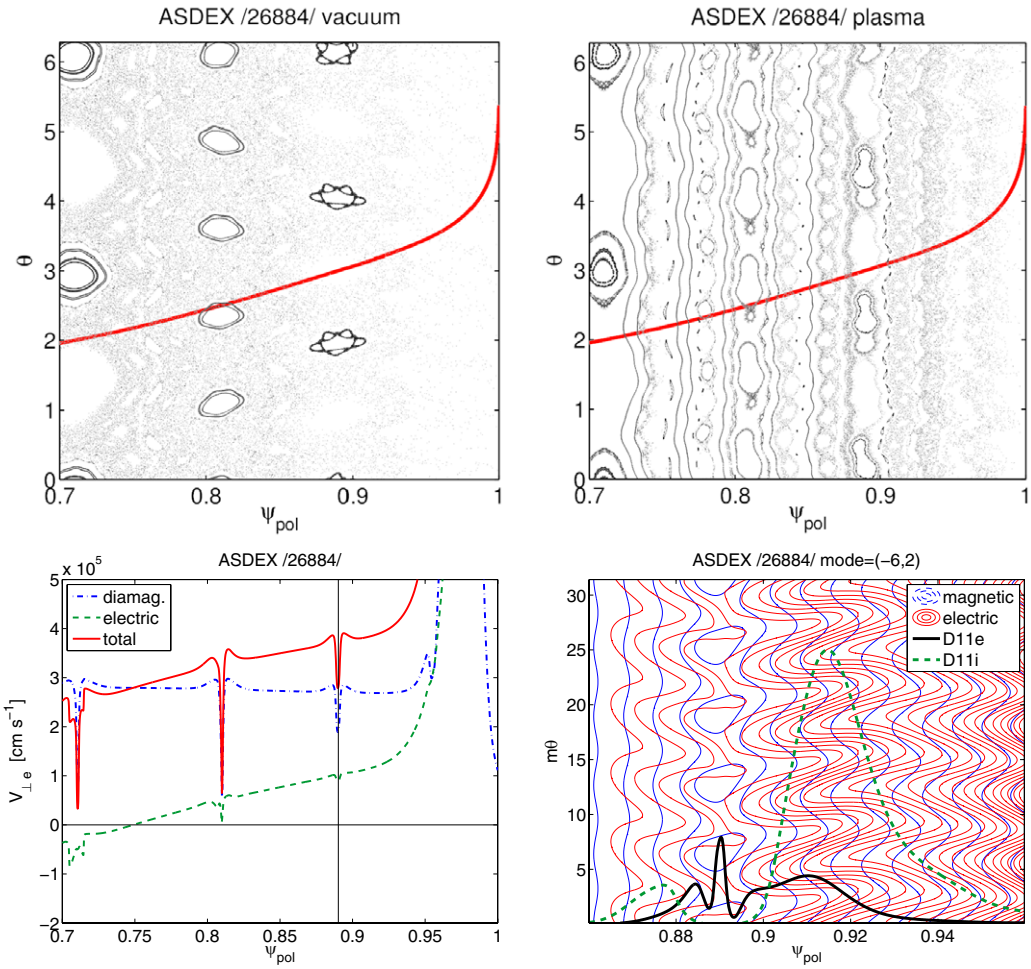

Figure 7. The same as figure 6 for shot 26884 and a separate mode $(-6, 2)$.

$D_{11}D_{22} - D_{12}^2 > 0$, the solution is $A_{1e} = 0$ and $A_{2e} = 0$. The second solution eliminates the electron temperature gradient, and the first means that the electric field in A_{1e} must be balanced by the density gradient. Partly this is done by a change in the toroidal rotation, but in the presence of shear viscosity the electric field does not relax to zero, and the density gradient must also change. The resulting density gradient is determined by the remaining electric field and can be even positive. Correspondingly, the change of the gradient can either be positive or negative. Actually, the possibility of such a steepening of the density gradient by RMPs has been reported earlier in non-linear MHD modelling in [33].

Finally, the last plots in figures 6–8 allow us to estimate the validity of the linear (quasilinear) model used in the present calculations. Linear (quasilinear) theory is valid if the non-linear wave–particle phase shift during the linear decorrelation time is small. This phase shift is caused by the radial particle displacement during its parallel motion (convective or diffusive, depending on the regime) along the perturbed field lines. This type of applicability condition is formally the same as the condition that the radial width of the quasilinear diffusion coefficients (it is the same as the width of the parallel response current) is smaller than the island width. The electron and ion quasilinear coefficients shown there for the single mode (indicated by the vertical line in the perpendicular velocity plot) using the same abscissa have approximately the same width as the islands, and, therefore, the approximation of this paper is marginally valid. The applicability condition, however, is violated for the largest in amplitude modes in shot 26884 (not shown here) where the bulk plasma performance is affected by the RMPs.

4. Equilibrium electric field reversal

In order to study the role of resonances connected with the perpendicular rotation of the plasma components, model polynomial plasma parameter profiles shown in figure 9 (these profiles roughly represent profiles in ASDEX Upgrade shot 26201) are used, and a scan over the toroidal velocity by scaling is performed for mode $(m, n) = (-10, 2)$. The dependences on the V_z scaling factor are equivalent to the frequency dependences usually used in such scans [6, 9]. The dependence on the V_z scaling factor of the form factor module $|T_{-10,2}|$ (see (75)) at the resonant surface is shown in the left plot of figure 10. Two maxima of field penetration, as follows from the plot on the right of figure 10, can be associated with the zero of the electron fluid velocity $V_{\perp e} = 0$ (right maximum) and with the reversal of the equilibrium radial electric field, $\partial\Phi_0/\partial r = 0$ (left maximum). The former resonance is a collective effect because no particular changes occur in Green's

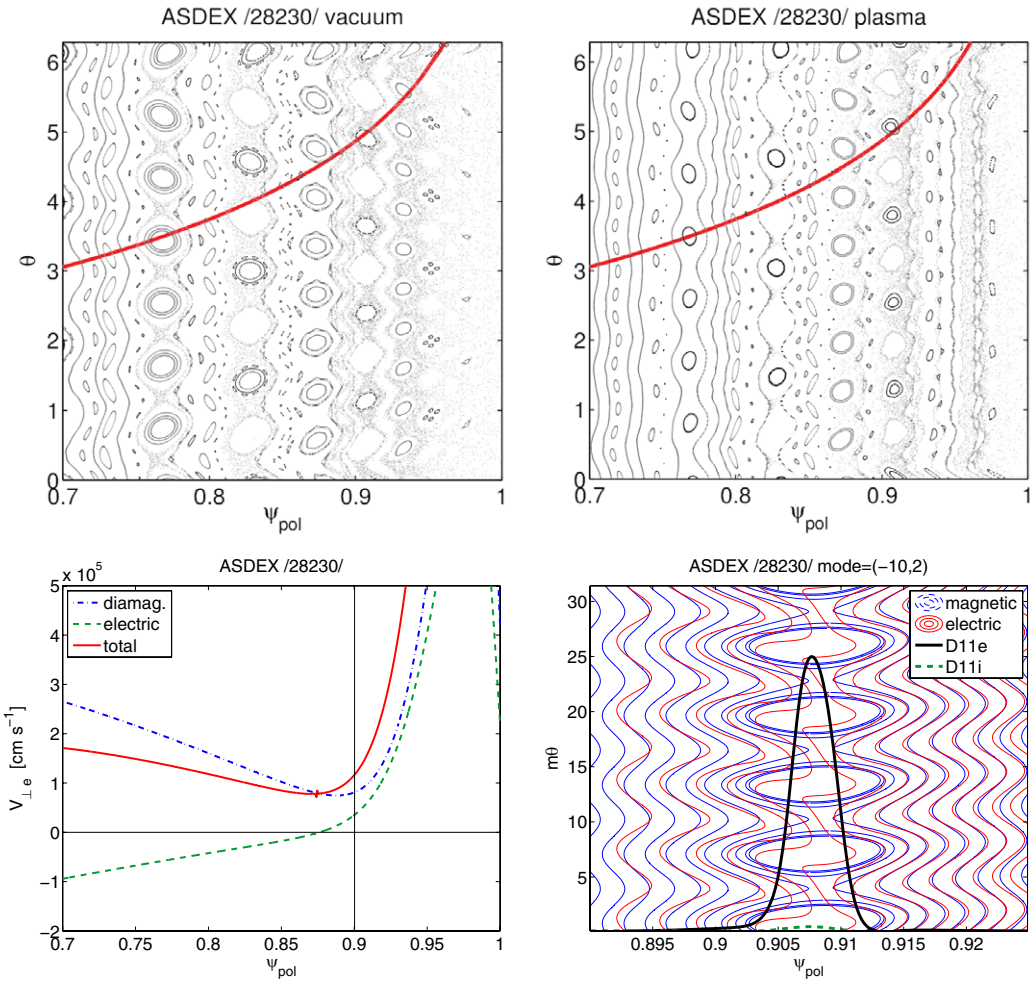

Figure 8. The same as figure 6 for shot 28230 and a separate mode (−10, 2).

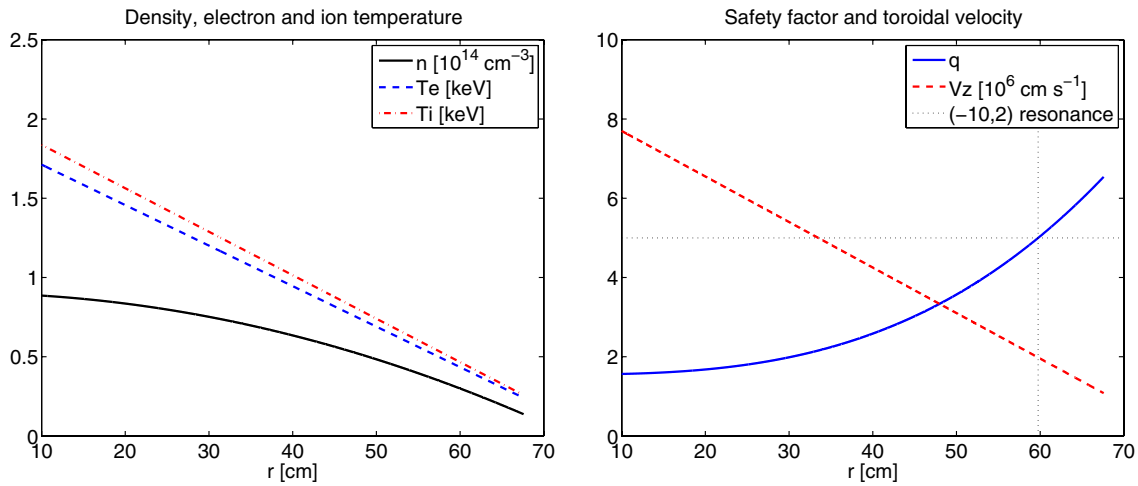

Figure 9. Model plasma parameter profiles: linear temperature and quadratic density profiles (left), cubic safety factor and linear toroidal velocity profile (right).

function representing the unperturbed particle motion, rather a special relation between the thermodynamic forces is fulfilled. The latter resonance is essentially a particle resonance because Green's function becomes singular when the electric field reversal point coincides with the resonant surface radius. In this case both, the $k_\parallel$ and ω_E vanish on the left-hand side of equation (30), and there is no other mechanism that can decorrelate particles and the perturbation field. Collisions do

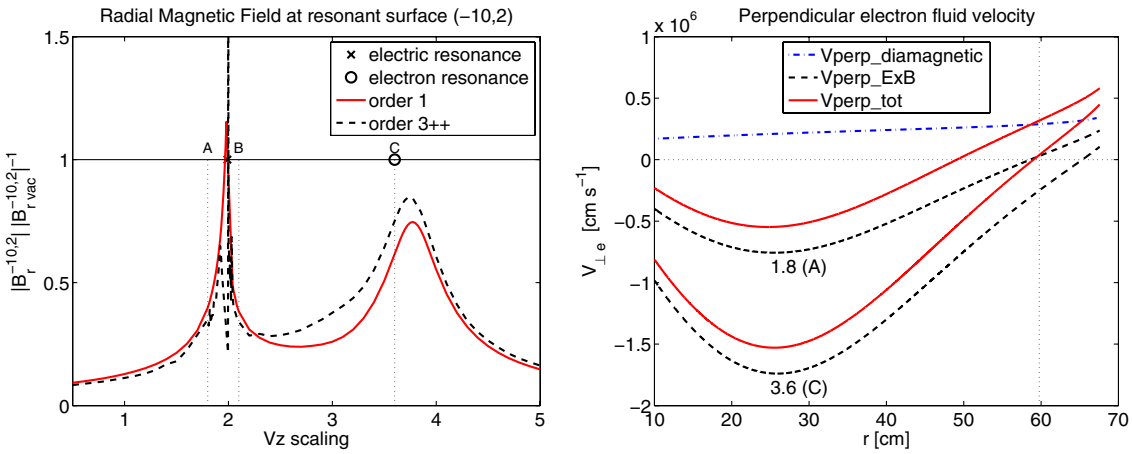

Figure 10. Left: scaling with V_z of the radial magnetic field amplitude B_r at the resonant surface for mode $(-10, 2)$. First-order Larmor radius expansion (solid) and third order Larmor radius expansion (dashed). Right: perpendicular electron diamagnetic (dotted), electric (dashed) and total (solid) velocity for scaling factors 1.8 and 3.6.

not remove this singularity in the lowest moment I^{00} describing density transport by $\boldsymbol{E} \times \boldsymbol{B}$ drift what can be checked by integrating (30) over $v_\parallel$. As a result of this integration, the left-hand side of (30) vanishes but, in general, not the right-hand side. This singularity cannot be removed by particle transport within the flux surface (in particular not by including magnetic drifts) and is removed either by non-linear effects or by some cross-field transport, which is not taken into account in the present model.

It should be noted that the first-order standard expansion model has actually been verified in this study by a 3++ expansion scheme (see section 2.2). The result of the 3++ model is shown as a dashed line in the left plot of figure 10 and stays in agreement with the standard model.

Remarkable is the behaviour of total torques given for individual species by integrals of torque densities (67) over the volume:

$$T^{(\mathrm{tot})}_{\varphi(\mathrm{e,i})} = \int_0^a \mathrm{d}r S T^{(\mathrm{EM})}_{\varphi(\mathrm{e,i})}, \tag{78}$$

with S being the flux surface area. The total electron torque can also be used as a measure of the radial particle transport. It can be seen from figure 11 that in the case of electron fluid resonance $V_{\perp \mathrm{e}} = 0$ as, or better to say always when RMPs are shielded, the torque is dominated by electrons. The sum of individual torques then is the same as the electron torque, and that means that together with increased particle transport toroidal plasma rotation should also change visibly.

In turn, when approaching the electric field reversal point, both torques increase approximately in the same manner, and this increase is even larger than the increase in the electron torque near the electron fluid resonance $V_{\perp \mathrm{e}} = 0$. However, the signs of the torques are opposite, and they largely balance each other to give a small total torque. As a consequence, the increase in particle transport need not be accompanied by a change in toroidal rotation, because induced particle fluxes are ambipolar, and do not charge the plasma. The reason for the rise of such an ambipolar transport can be understood from the remaining plots in figure 11. The contours of the perturbed electrostatic potential are perturbed very weakly in the case of electron fluid resonance (point C) where the main transport is due to parallel streaming of electrons along the perturbed field lines. However, equipotentials are strongly perturbed near the electric field reversal point.

It can be seen that for the case of point B convective cells are formed. Such cells have been reported in [14]. Since the transport in these cells is the $\boldsymbol{E} \times \boldsymbol{B}$ drift, the transport is independent of particle charge and mass and therefore is ambipolar. Note that the formation of such cells is a mere result of the fact that the electric field reversal point is also an electrostatic potential extremal point. Even weak perturbations of the potential cause, around the extremal point, formation of 'islands' similar to the formation of islands on the perturbed magnetic flux contours (magnetic islands). It should also be noted that potential contours, which are non-aligned with perturbed magnetic surfaces, are observed only on one side of the electric field reversal point, in the region between this point and the electron fluid resonance point. According to [34], drift waves are excited in this region. The drift wave domain discussed there is between the zeros of the total electron and total ion fluid velocities, which is formally different from the domain observed in this paper. However, no contradiction arises because the ion temperature is set to zero in [34] and ion fluid zero in these circumstances cannot be distinguished from the electric field reversal point.

As one could have noticed from figure 9 the radial magnetic field does not simply return to the vacuum value in the electric field reversal point, but is even amplified there. Actually, experimental measurements of divertor flux splitting by the RMPs in DIII-D brought the authors to the conclusion that the RMP field could have been amplified by the plasma [35]. The field amplification seen in this study could be responsible for this effect.

Finally, it is important to estimate the role of anomalous transport, which is not taken into account in the present model. It has been reported in [9] that even a small amount of the anomalous transport eliminates all fluid resonances except for the electron fluid resonance $V_{\perp \mathrm{e}} = 0$. Actually the ion fluid resonance has never been observed for the kinetic model of this paper. As for the resonance near the electric field reversal point reported here, the role of anomalous transport

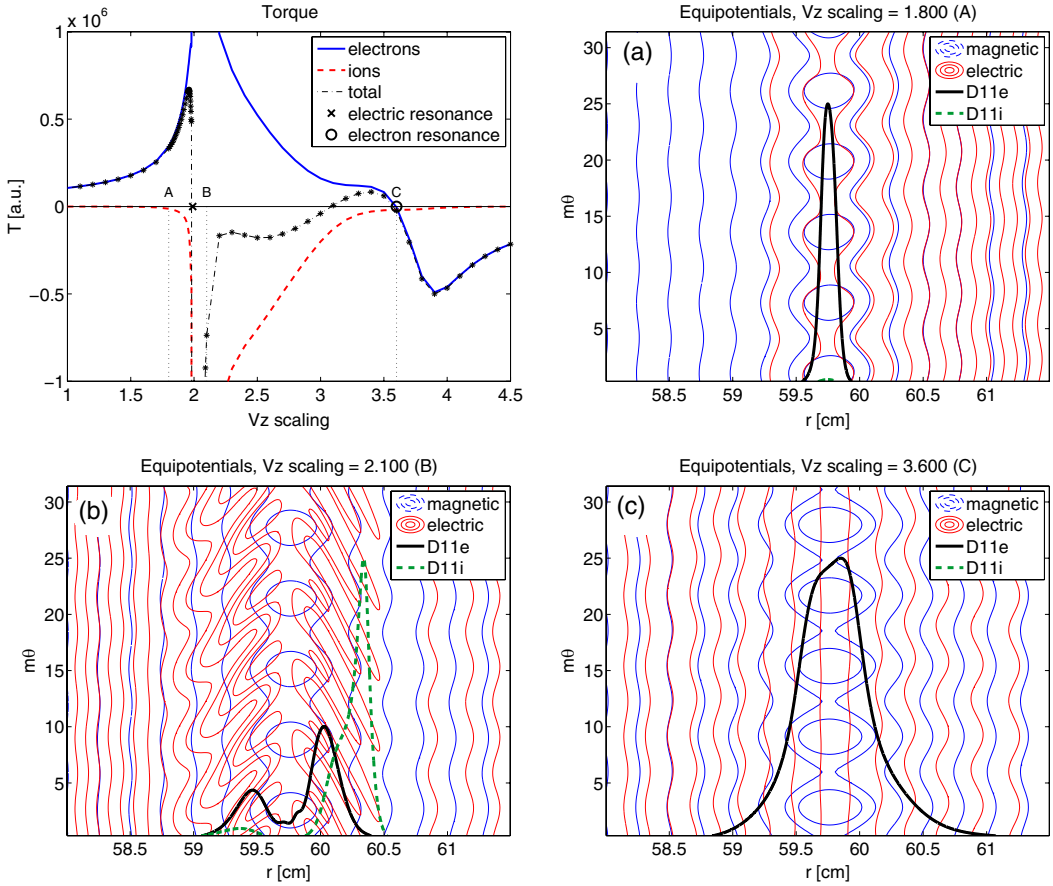

Figure 11. Torque acting on electrons (solid) and ions (dashed) and total torque (dashed–dotted) for linear-parabolic tokamak-like profiles. Magnetic and electric equipotential surfaces as well as electron (solid) and ion (dashed) D_{11} diffusion coefficients for different V_z scalings (*a*), (*b*) and (*c*) indicated by vertical lines in the upper-left plot.

can be estimated in the following way. The decorrelation rate provided by the anomalous diffusion can be estimated as $\nu_{\text{eff}} = D_\perp \Delta r^{-2}$ where Δr is the resonant layer half-width (roughly the half-width of the electron diffusion coefficient D_{11}). Estimating this width as 0.25 cm from figure 11 and using equation (77) one obtains $\nu_{\text{eff}} \sim 8 \times 10^4\,\text{s}^{-1}$. Estimating now $k_\parallel \approx k_z q' q^{-1} \Delta r \sim 10^{-4}\,\text{cm}^{-1}$ more accurately than above one obtains for electrons with $T_e \sim 0.5\,\text{KeV}$ that the parallel decorrelation rate (Doppler frequency shift) is $k_\parallel v_\parallel \sim 10^5\,\text{s}^{-1}$, i.e. the effect of the anomalous transport is significant but not dramatic. The reason for the somewhat exaggerated role of anomalous transport in the two-fluid MHD theory is the rather narrow width of resonant layers reported in [9] to be five times narrower than the ion Larmor radius. Since the decorrelation rate scales inversely with the square of the resonant layer width, this rate is overestimated by more than an order of magnitude compared with the kinetic width, which is usually about the ion Larmor radius in low-collisionality plasmas.

5. Conclusions

The comparison of several first ASDEX Upgrade shots with DIII-D shot 126006, which has a significantly smaller plasma collisionality, shows a rather different behaviour of the RMPs in the plasma. In contrast to the DIII-D shot, where the strong shielding of most of the perturbation spectral modes prevents the formation of an ergodic layer, the shielding of the perturbations in ASDEX Upgrade is rather weak—by a factor ten or even less. Such a weak shielding does not prevent the formation of an ergodic layer but rather reduces the size of the ergodic layer to approximately the size of the pedestal region. The optimum performance is achieved in ASDEX Upgrade when this layer simply covers the whole pedestal while a wider layer leads already to a degradation of the electron temperature.

The ELM mitigation mechanism for such high-collisionality scenarios appears to be the same as the mechanism originally considered by the authors of the method—reduction of the pedestal pressure due to an enhanced transport in the ergodic field [1]. This conclusion is based, in the present context, more on the assessment of the ergodic layer size rather than on the results of the cylindrical transport model which shows rather small, a few per cent change of the pedestal pressure. However, the cylindrical model is not accurate near the sepratrix, and this conclusion should still be verified by more suitable tools such as the 3D transport code E3D [10, 36]. The choice in favour of an ergodic layer width is because it is less sensitive to errors in the mode amplitude computed by the linear code (the Chirikov criterion scales as the square root of the mode amplitude) while the quasilinear coefficients are quadratic in this amplitude and therefore much more prone to errors. Basically, the properties of the shielded ergodic layer

are pre-determined by the properties of the ergodic layer in vacuum and the main role is not played by the modes resonant in the core plasma (these modes rather have a deleterious effect) but by the modes resonant in the pedestal. Since the magnetic shear is high in the pedestal, spectral modes with relatively low amplitudes but high poloidal mode numbers are required because the Chirikov overlapping criterion scales as a square root of the amplitude but linearly with the poloidal number. In order to fulfil the resonance conditions for high poloidal mode numbers, higher toroidal numbers are desirable that are not commensurable between each other. In the present ASDEX Upgrade experiments the main toroidal mode number was $n = 2$. This is lower than that in DIII-D and is closer to the experiments on JET where higher toroidal numbers were hardly achievable due to the limitation of the coil design.

As shown recently in [9, 14] the ELM mitigation mechanism is quite different in low-collisionality discharges. In this case, instead of formation of the ergodic field region, a few or even a single mode of the spectrum is resonant—the mode which is close to one of the fluid resonances (electron fluid resonance $V_{\perp e} = 0$ in case of [9, 14]). Such a resonance explains the narrow window of plasma parameters where ELMs are mitigated in the experiments.

In this paper it is shown that another fluid resonance, the equilibrium electric field reversal resonance $E_r = 0$ can also be responsible for the ELM mitigation with a similar narrow parameter window. The reason why this resonance has been ruled out in [9] is probably connected to the fact that the role of the anomalous radial transport is somewhat overestimated in two-fluid MHD theory and, therefore, this transport may in reality be not so deleterious for this resonance. At least, as shown in this paper, this resonance is not as strongly affected by anomalous transport in a collisional plasma with parameters close to ASDEX Upgrade parameters in the currently discussed discharges. It should be noted that according to [13] the $E_r = 0$ point is also present in the DIII-D shot 126006 and is located within the pedestal region. Actually, an enhanced transport in the region with strong density gradient pertinent to the pedestal would have a stronger effect on the plasma parameters. In particular, it would cause a stronger density pump-out than a resonance at the pedestal top where the gradients are smaller. An additional argument in favour of this resonance comes from the observations of amplification of the RMPs in relevant experiments. Such an amplification is also demonstrated in the current numerical modelling.

It should be noted that the conditions for an optimal use of fluid resonances are actually the same as the conditions for ergodic layer formation in the pedestal. Since those resonances are rather narrow in parameter space, the coil spectrum must be rather dense, and it is not so important that the amplitudes of the resonant modes are high. This requirement is similar to the requirement in the formation of ergodic magnetic field layers: small distances between the resonant surfaces are more important than amplitudes because the non-resonant modes are shielded by two orders of magnitude and are practically eliminated from the spectrum.

Thus, a preferable perturbation spectrum is achieved if many relatively high toroidal mode numbers, which are not commensurable with each other, are excited such that they provide the maximum possible density of resonances in the pedestal region. On the other hand, due to high values of the safety factor in the pedestal, very high toroidal mode numbers lead to even higher poloidal mode numbers in order to be resonant there. Those modes are already strongly attenuated by the vacuum opacity barrier, i.e. the amplitude scales with the poloidal mode number as $r^{|m|-1}$. Thus, a compromise is needed between the requirement of a dense spectrum and attenuation in such a barrier.

Acknowledgments

The authors are grateful to Per Helander for pointing out that the gyrokinetic approach can be useful in this problem and to Ilon Joseph for pointing out that shift of the electron fluid resonance corresponds to the neoclassical plateau regime.

This work, supported in part by the European Commission under the contract of Associations between EURATOM and the Austrian Academy of Sciences, was carried out within the framework of the European Fusion Development Agreement. The views and opinions expressed herein do not necessarily reflect those of the European Commission.

References

[1] Evans T.E. *et al* 2004 *Phys. Rev. Lett.* **92** 235003
[2] Liang Y. *et al* 2007 *Phys. Rev. Lett.* **98** 265004
[3] Becoulet M. *et al* 2008 *Nucl. Fusion* **48** 024003
[4] Suttrop W. *et al* 2011 *Phys. Rev. Lett.* **106** 225004
[5] Suttrop W. *et al* 2011 *Plasma Phys. Control. Fusion* **53** 124014
[6] Heyn M.F., Ivanov I.B., Kasilov S.V. and Kernbichler W. 2006 *Nucl. Fusion* **46** S159
[7] Ivanov I.B., Heyn S.V., Kasilov M.F. and Kernbichler W. 2011 *Phys. Plasmas* **18** 022501
[8] Heyn M.F. *et al* 2013 *Problems of Atomic Science and Technology* (*Plasma Physics Series 1*, vol 83) (Amsterdam: North Holland) p 51
[9] Waelbroeck F.L. *et al* 2012 *Nucl. Fusion* **52** 074004
[10] Joseph I. *et al* 2008 *Nucl. Fusion* **48** 045009
[11] Heyn M.F. *et al* 2008 *Nucl. Fusion* **48** 024005
[12] Fitzpatrick R. and Hender T.C. 1991 *Phys. Fluids* B **3** 644
[13] Joseph I. 2012 *Contrib. Plasma Phys.* **52** 326
[14] Nardon E. *et al* 2010 *Nucl. Fusion* **50** 034002
[15] Nardon E., Bécoulet M., Huysmans G. and Czarny O. 2007 *Phys. Plasmas* **14** 092501
[16] Yu Q., Günter S. and Finken K.H. 2008 *Nucl. Fusion* **48** 024007
[17] Littlejohn R.J. 1983 *J. Plasma Phys.* **29** 111
[18] Shaing K.C., Sabbagh S.A. and Chu M.S. 2010 *Nucl. Fusion* **50** 025022
[19] Park J., Boozer A.H. and Menard J.E. 2009 *Phys. Rev. Lett.* **102** 065002
[20] Ivanov I.B., Kasilov S.V., Kernbichler W. and Heyn M.F. 2007 *JETP Lett.* **86** 364
[21] Mulec M., Ivanov I.B., Heyn M.F. and Kernbichler W. 2012 *Phys. Plasmas* **19** 032502
[22] Nemov V.V., Kasilov S.V., Kernbichler W. and Heyn M.F. 1999 *Phys. Plasmas* **6** 4622
[23] Hirshman S.P. 1978 *Nucl. Fusion* **18** 917
[24] Hinton F.L. and Hazeltine R.D. 1976 *Rev. Mod. Phys.* **48** 239
[25] Helander P. and Sigmar D.J. 2002 *Collisional Transport in Magnetized Plasmas* (Cambridge: Cambridge University Press)
[26] Kernbichler W. *et al* 2008 *Plasma Fusion Res.* **3** S1061
[27] Heyn M.F. *et al* 2008 *35th EPS Conf. on Plasma Physics (Hersonissos, Greece, 9–13 June 2008)* vol 32D (ECA) (Mulhouse: European Physical Society) pp P-5.009
[28] Heyn M.F. *et al* 2012 *Nucl. Fusion* **52** 054010

[29] Furth H.P., Rutherford P.H. and Selberg H. 1973 *Phys. Fluids* **16** 1054
[30] Shaing K.C. 2001 *Phys. Rev. Lett.* **87** 245003
[31] Cole A. and Fitzpatrick R. 2006 *Phys. Plasmas* **13** 032503
[32] Joseph I. *et al* 2007 *J. Nucl. Mater.* **363–365** 591
[33] Yu Q. and Günter S. 2009 *Nucl. Fusion* **49** 062001
[34] Militello F. and Waelbroeck F.L. 2009 *Nucl. Fusion* **49** 065018
[35] Jakubowski M.W. *et al* 2009 *Nucl. Fusion* **49** 095013
[36] Runov A.M. *et al* 2001 *Phys. Plasmas* **8** 916